Title

MEASUREMENTS OF ELECTRICAL CONDUCTIVITY FOR CHARACTERIZING AND MONITORING NUCLEAR WASTE REPOSITORIES

Authors

Morrison, H.F.
Becker, A.
Lee, K.H.

Publication Date

1986-11-01

Lawrence Berkeley Laboratory
UNIVERSITY OF CALIFORNIA

EARTH SCIENCES DIVISION

MEASUREMENTS OF ELECTRICAL CONDUCTIVITY FOR CHARACTERIZING AND MONITORING NUCLEAR WASTE REPOSITORIES

H.F. Morrison, A. Becker, and K.H. Lee

November 1986

Prepared for the U.S. Department of Energy under Contract DE-AC03-76SF00098

DISCLAIMER

LBL-22641

Measurements of Electrical Conductivity for Characterizing and Monitoring Nuclear Waste Repositories.

H.F. Morrison, A. Becker and K.H. Lee

Materials Science and Mineral Engineering

and Earth Sciences Division

Lawrence Berkeley Laboratory

University of California

Berkeley, California 94720

November 1986

This work was supported by the Assistant Secretary for Energy Research, Office of Basic Energy Sciences, Division of Engineering and Geosciences of the U.S. Department of Energy under Contract No. DE-AC03-76SF00098.

Table of Contents

1. Introduction

The siting and future integrity of nuclear waste repositories is critically dependent on the groundwater regime in the area. The site must be located far from high permeability acquifers and the state of the water in the vicinity of the site must be monitored after waste emplacement to detect changes in the groundwater flow that might have been caused by the excavation itself or by the subsequent heating of the rocks by the waste. The effectiveness of dewatering techniques, grouting-off water filled fracture zones, etc. must be closely monitored in the early stages of repository evaluation. Longer term changes associated with regional effects, climate changes or even tectonic forces must be monitored with some sort of a reliable and safe technique that does not require reentry or even access to the repository itself.

Geophysical techniques offer promise in achieving the goals of monitoring the physical properties of the rocks in the vicinity of the repository. Electrical methods seem particularly promising in monitoring the groundwater regime since the electrical conductivity of rocks depends almost entirely on the pore water content. Thus the bulk resistivity depends on the porosity (including fracture porosity), saturation, dissolved solids in the pore water, and temperature. These factors cannot be isolated in a resistivity measurement. If geological controls, groundwater measurements or other geophysical methods are employed, electrical methods can be used to detect zones of varying water content and, most importantly for this study, to monitor time changes in the rocks associated with changing saturation, temperature, etc.

The detection of major fractures is one topic of this study but another equally important problem is to develop quantitative relationships between large scale resistivity and fracture systems in rock. There has been very little work done on this central issue. Empirical relations between resistivity and porosity have been derived on the basis of

laboratory samples or from well logging, but there are no comparable 'laws' for rock masses with major fracture or joint patterns. Hydrologic models for such rocks have recently been derived but the corresponding resistivity models have not been attempted. Resistivity due to fracture distributions with preferred orientation could be determined with such models, as could quantitative interpretation of changes as fracture aperture varies with load. This study is not only important for the assessment of a repository site, but has far ranging implications in reservoir studies for oil, gas, and geothermal resources.

The electrical conductivity can be measured in two ways. Current can be injected into the ground through pairs of electrodes and corresponding voltage drops can be measured in the vicinity with other pairs of electrodes. In general, electrodes can be used in the subsurface although traditionally the arrays have been employed on the surface. Measurements of voltage and current for different electrode geometries are then used to infer the subsurface distribution of conductivity. These methods are indirect but ideally suited to measure the properties of a region to which it is impossible to gain direct access. The resulting interpretation of the conductivity distribution is not unique, nor does it provide high resolution of subsurface features. In many applications this latter property is to our advantage since the measurements yield bulk average values of the conductivity which often includes features that are not included in hand sample or borehole logging measurements (e.g. fracture porosity).

The uniqueness property of the interpretation is only now yielding to quantitative analysis. It depends on the geometry used in the survey. For simple horizontal layers the uniqueness and resolution is quite well understood. In inhomogeneous media the uniqueness problem has only been addressed by cumbersome trial and error experiments using numerical forward models to match field data by successive iterations.

Recently we have attempted to quantify this process by using rigorous generalized least squares inversion techniques and this promises to greatly speed up interpretation and at the same time quantify the uniqueness question.

The electrical conductivity can also be measured inductively. Instead of injecting current into the ground as described in the dc resistivity method above, currents can be induced to flow by a changing magnetic field. The source of the changing magnetic field could be a loop of wire carrying alternating current, or, again, a wire grounded with electrodes in which alternating rather than direct current is used. The currents induced in the ground are measured either by detecting the magnetic fields they produce or by measuring the voltage drops in pairs of electrodes. Sources and receivers can be on the surface, in the ground, or combinations of both.

In these inductive or electromagnetic (em) methods the interpretation depends both on transmitter-receiver geometry and frequency of operation. In principle the interpretation should be more definitive than with the dc resistivity methods. Rigorous confirmation of this statement in inhomogeneous media awaits the development of generalized inversion techniques for em methods.

The em methods offer some proven advantages over the dc methods. Measurements can be made without contacting the ground; measurements are insensitive to high resistivity zones; depth of investigation can be controlled by the frequency of operation so that large transmitter-receiver spacings are not required; and because of the transmitter source field fall-off, the methods are not sensitive to conductivity inhomogeneities far from the zone of interest.

Both electrical and em methods are applicable in mapping and monitoring waste repository sites. Recent developments in mathematical

modelling, generalized inversion, and field techniques and instrumentation, have combined to offer a quantitative approach to such monitoring that is not only non-invasive but highly diagnostic of the properties of the site and its post-emplacement changes. There are two stages for further research on these topics:

I. Mapping the subsurface resistivity distribution prior to and during the excavation and preparation of the site. This would include determining the general resistivity distribution which will be the starting point for the long term monitoring and will also include measurements to locate specific fractures or fracture zones which may be in the vicinity of the site but not detected in drilling or excavation.

II. Monitoring the subsurface resistivity changes associated with site excavation and preparation and long term changes after waste emplacement and repository closure.

A parallel and integral study of the basic relationship between fractures and resistivity in rock is also required. The results of this study would then be used in the design of the experiments to map and monitor the in situ resistivity.

2. Electrical Conductivity of Rock

The electrical conductivity of rocks and unconsolidated sediments in the upper few km of the earth's crust is governed by the water content and the nature of the water paths through the rock. Electrical current is carried by ions in the water and so the bulk resistivity will depend on the ionic concentration and ionic mobility as well as the saturation and nature of the porosity. The dependence of the conductivity on temperature and pressure is due to the change in ion mobility with temperature and the effect of pressure on the apertures of the pore paths respectively. The presence of clays in a rock has a large effect on

the conductivity because of the increased ion concentration in the diffuse layer adjacent to the clay mineral surface. In fact, such a phenomenon occurs at all mineral surfaces but to a lesser extent than with highly surface active minerals like clay. The surface conduction mechanism is important in understanding the behavior of partially saturated rocks and also in setting limits on the extent to which electrical conductivity can be linked to hydraulic conductivity.

Most studies on the electrical conductivity of rocks have been on sedimentary rocks because of their importance in petroleum exploration and well logging. Archie (1942, 1947) established an empirical relationship between the formation resistivity (ρ_0) the pore fluid resistivity (ρ_w) and the porosity φ which is now referred to as Archie's Law :

$$\rho_0 = a\rho_w \varphi^{-m}$$

where a and m are constants for a given rock. For a very wide range of sedimentary rocks and for some volcanic and intrusive rocks as well, the constant, a, is close to unity and m is close to 2.0 (Keller and Frischknecht, 1966). Surprisingly there has not yet been a theoretical model advanced to explain this inverse dependence of resistivity on the square of porosity.

An important and little studied aspect of rock conductivity is the role of fractures on the resultant bulk properties. Laboratory studies concentrate on small samples which almost by definition do not include fractures or joints. Field studies using surface resistivity measuring arrays are usually too strongly influenced by the inhomogeneous nature of a particular rock unit to allow fracture and pore porosity to be separated. With the increased measurement accuracy and resolution provided with subsurface techniques and the interest in monitoring time changes in resistivity, it is essential to investigate more closely the role of fracture porosity on the electrical conductivity of large rock masses.

It is well known that the hydraulic conductivity or permeability is strongly influenced by the fracture distribution : excellent numerical models are now available for characterizing fluid flow in fractured rock (e.g. Long and Witherspoon, 1985). It is also known that seismic velocities are also strongly affected by fractures in the rock. It remains to develop expressions for the electrical conductivity of such rocks and to take advantage of this valuable physical property for characterizing and monitoring large subsurface volumes of rock. In the following paragraphs we will summarize what little work has been done on the role of fractures in rock conductivity.

The simplest model of a fractured or jointed rock is one in which the fractures are plane parallel thin layers of conductivity σ_1 in a rock mass of conductivity σ_2. Grant and West (1965) showed that for this model, shown with appropriate axes in Figure 1, the conductivity in the direction parallel to the fractures (σ_x or σ_y) was given by :

$$\sigma_x = \sigma_y = p\,\sigma_1 + (1-p)\sigma_2$$

where p is the volume fraction of this fracture. If we assume that the rock matrix conductivity, σ_2 , is governed by the simple form of Archie's law, i.e.

$$\sigma_2 = \sigma_w \varphi^2$$

and if we further assume that the conductivity of the pore fluid in the rock matrix , σ_w, is in fact the same as the conductivity of the fluid in the fracture, σ_1, then we can substitute $\sigma_1 = \sigma_2 / \varphi^2$ in the above expression for σ_x and we obtain

$$\sigma_x = p\frac{\sigma_2}{\varphi^2} + (1-p)\sigma_2$$

or

$$\frac{\sigma_x}{\sigma_2} = \frac{p}{\varphi^2} + (1-p)$$

This immediately reveals that a very small fracture porosity can have a dramatic effect on the conductivity of the rock. For example if the fracture porosity is 0.005 and the rock matrix porosity is 0.05 the conductivity in the direction of the fractures is 3 times the rock resistivity. In general if p << 0.1, and φ < 10 p, $\sigma_x / \sigma_2 \approx p / \varphi^2$. Figure 1 shows the relationships of σ_x / σ_2 to p and φ. If the rock porosity is zero the above expression must be rewritten to simply show that $\sigma_x = p\,\sigma_1$ since σ_2 is zero.

Keller and Frischknecht (1966) derived an expression for the resistivity of a rock with a totally random pattern of fractures with a volume fraction of p as :

$$\rho_0 = 2.46 \rho_w p^{-1}$$

or

$$\sigma_0 = \sigma_w \frac{p}{2.46}$$

where it was assumed that the fractures were the only porosity. The random pattern of fractures reduces the conductivity by a factor of 2.46 over the model in which all the fractures are parallel.

Fractures clearly introduce anisotropy in a rock and in some situations even small fracture porosity can greatly alter the rock resistivity. There apparently has been no work to develop resistivity expressions for the hydraulic conductivity models in which fracture distribution size, aperture and interconnectedness are all taken into account. Hoeing (1979) determined the 'effective' electrical properties of a medium with randomly distributed elliptical cracks, and Greenberg and Brace (1969) and Sharkland and Waff (1974) used network models to characterize saturated rocks and to simulate a decrease in porosity brought about by fracture closure.

That fractures do play an important role in rock resistivity is practically demonstrated in the work by Brace and Orange (1966, 1968a, 1968b). Figure 2 summarizes their work on the effects of confining pressure on the resistivity of a water saturated granite. At low pressures the resistivity increases as the confining pressure increases and Brace et al. attribute this effect to the closure of fracture porosity. In Figure 2 it is seen that the resistivity increases by a factor of 10 as the pressure increases to 400 Mpa. From our fracture analysis above this could easily be explained by the disappearance of only 0.1% fracture porosity in a granite of 1.0% pore porosity.

3. Mapping of Subsurface Conductivity Distribution

A. DC Methods

Surface current and potential electrode arrays have been used for many years to determine the subsurface resistivity. Excellent reviews of the theory and practice of these methods are presented by Van Nostrand and Cook (1966), Grant and West (1965), Keller (1966), and Keller et al. (1975) to name only a few. The most important recent development in surface schemes is the use of two and three dimensional numerical models to represent the ground in interpreting the data. Beyer (1977) conducted an exhaustive analysis of over 200 km of dipole-dipole date taken in profiles over geothermal prospects in Nevada. He used a two dimensional finite difference modelling algorithm developed by Dey and Morrison (1976) to interpret this data. While these analyses yielded models that are in excellent agreement with geological and other geophysical data, there has been very little work done on the uniqueness of the interpretation. This problem has been attacked by Sasaki (1982) using an improved version of the Dey (1976) algorithm to obtain generalized least squares inversion models of field data. This approach

promises to be very effective in interpreting surface and subsurface data, and more importantly it will finally allow quantitative estimates of the uncertainty in the model representing the ground. This will be essential in interpreting surveys of waste repository sites.

Resistivity mapping using subsurface electrodes permits far greater accuracy and resolution than can be obtained with surface-only arrays. Alfano (1962), Merkel (1971), and Snyder and Merkel (1973) developed solutions for the potential distribution on the surface of a layered medium for a buried current source. Daniels (1977, 1978) discussed in detail anomalies due to spherical bodies and for an n-layered earth for the cross-hole and borehole-to-surface array configurations. Field applications of these techniques were presented in Daniels (1983) and Dyck (1984). Theoretical solutions for apparent resistivity anomalies due to spheres and oblate and prolate spheroids were discussed in Dobecki (1980), Lytle (1982), and Lytle and Hanson (1983). Yang and Ward (1985a, 1985b) and Beasley and Ward (1986) presented the results of sensitivity analyses of thin ellipsoids, spheroids, and plate-like bodies (simulating fracture zones) by single and cross-hole arrays using integral equation techniques.

In the above investigations results were presented as normalized apparent resistivity (ρ_a/ρ_1) (as is standard with conventional surface resistivity data) or were displayed on plan-view apparent resistivity contour maps. While the evidence usually indicated that an anomalous body is detectable by downhole techniques, accurately describing the location and geometry of the body still seems remote. Beasley and Ward (1986) found that when the source electrode is above, below, or to the side of a thin body the calculated apparent resistivities were basically the same. Thus a method needs to be developed which can clearly delineate the location, depth, and geometry of an anomalously conductive or resistive body.

An important step in this study has been the introduction of subsurface sources in the numerical models. We have modified the 2-D and 3-D code of Dey and Morrison (1976 and 1979 respectively) so that hole-to-surface and hole-to-hole electrode arrays can be studied. The programs have already been used in a subsurface contaminant study and a powerful differencing technique has been discovered which greatly assists the interpretation.

Wilt et al. (1983) used the 3-D program to model an idealized geothermal reinjection process, and later Wilt and Tsang (1985) used the same program to simulate subsurface contaminant migration. In a field study of contamination from leaking evaporation ponds Asch et al. (1986) have used a subsurface to surface survey to locate the anomalous conductivity caused by high salinity water invading an acquifer beneath the pond.

In the surface and subsurface arrays the results are presented in terms of the apparent resistivity : the resistivity of a uniform half space that would have given the observed potential difference for that specific electrode geometry and current. We have used a highly idealized model of a waste repository to illustrate the apparent resistivity maps produced by a variety of arrays.

The model is shown in Figure 3. We have assumed that in excavating and preparing the repository the water content of the rocks has been reduced so that the effective resistivity of a 100 m thick zone has increased by a factor of three over the normal or background value (in this case 200 ohm m).

In Figure 4a the results of a standard dipole-dipole surface survey are presented for the model in Figure 3. The data in Figure 4b are the percent differences observed in the apparent resistivity relative to the 200 ohm m half space. The anomaly is diffuse and broad but quite large

enough to be detected; for time monitoring with fixed surface electrodes the sensitivity to small changes in the repository resistivity (eg. as water reentered the zone) would be quite high.

In Figure 5a the model is shown again, this time with a current electrode at various levels in an offset well. The apparent resistivities measured for a given depth of the current electrode and location of surface potential dipole electrodes are plotted in Figure 5b at the levels of the current electrode and beneath the potential electrodes. Again, in Figure 5c, the percent differences of the repository data with respect to the background resistivity (200 ohm m) are plotted. While not directly comparable with the dipole-dipole data taken on the surface this array does not seem to provide any diagnostic advantage over the surface array data.

In Figure 6a the same model is shown, this time for the case of a current electrode at various levels in a borehole penetrating the repository. Here (in Figure 6b) the percent difference anomaly relative to the halfspace resistivity is dramatic and very tight contours define the boundaries of the repository.

An equally dramatic definition of the repository boundaries is produced by using percent differences calculated, not in reference to the background halfspace resistivity, but compared to the apparent resistivities observed at a particular depth of the current source. An example is shown in Figure 6c in which all the apparent resistivities in the section are compared to the values observed with the source at 650 meters depth. Note that the differences are of slightly greater magnitude than those presented in Figure 6b.

Even more resolution can be obtained using subsurface dipole sources and surface receiver dipoles (Figure 7). As shown in the model (Figure 9a), the current electrodes are placed every 150 meters and and

are treated as a series of dipole sources. The much higher apparent resistivities (Figure 7b) obtained from having a dipole source straddling the repository and the resulting percent differences plotted in Figure 7c illustrate the greater sensitivity of downhole dipole sources (as compared to arrays confined to the surface) to changes in the resistivity distribution.

Figure 7d shows percent differences with the apparent resistivities from the shallowest subsurface dipole source (between the surface and 150 meters) used as the reference values. Note the similarities between this figure and the previous percent difference plot (Figure 7c) in which the halfspace resistivity was the reference value. The relationship exists because the first downhole dipole 'looks' at predominantly only the first 150 meters of the section and thus the resulting resistivities are quite close to the halfspace value. In contrast, if the resistivities from the dipole located at 600 to 750 meters (which straddles the repository) are the reference values, then the resulting percent difference anomaly is much larger and the repository zone is even more easily identified (Figure 7e).

The subsurface arrays also hold great promise for eliminating or reducing near-surface effects. The results of a surface dipole-dipole survey over the repository model with two small conductive bodies on the surface are presented in Figure 8a. The percent differences plot of this data (Figure 8b) is quite similar to the pseudo-sections having conductive surface bodies which were presented by Beyer (1977). Note that the effects of the surface conductors are observed throughout the section and make it very difficult to determine the deeper structure.

In Figure 9a the same model is shown for the case of the single downhole source and surface receiver dipoles. The percent differences calculated with the resistivity of the halfspace as reference are presented in Figure 9b. Note that the large anomalies directly under the

surface conductors again traverse the whole section as was the case for the surface dipole-dipole array (Figure 8b). The repository is still discernible but the entire picture is much more complicated by the conductors at the surface.

However, using the resistivities observed with the current source at 650 meters depth (inside the repository) as the reference values, the percent difference plot (Figure 9c) shows that the effects due to the surface conductors have been almost entirely eliminated. In fact, comparing this figure to Figure 6c in which no conductors were present, we see that they are almost identical except for the two anomalies near the surface in Figure 9c. This example illustrates the power of relative percent differencing to remove unwanted near-surface and topographic effects.

In summary, dc resistivity mapping with combinations of surface and subsurface electrodes appear to have great potential. Much work remains to be done in selecting the best array geometries for sensitivity in mapping features of interest in site studies.

A model study to design the optimum array for mapping and monitoring an actual repository site would include at least the following topics:

a) Current Source(s) in a central pillar and to the side (since it probably would not be possible to place the current electrodes directly in the repository).

b) Effects of near-surface variations in resistivity and topography in both hole-to-surface and hole-to-hole arrays.

c) Sensitivity of various arrays to changes in resistivity and thickness of the repository zone.

In 'c)' hydrologic and thermal heating models could be combined to yield the resistivity changes that could be expected for various scenarios such as water re-entry, heating, or even vaporization.

B. The Well Casing Problem

The resistivity methods discussed above, and the electromagnetic methods to be described are all strongly influenced by the presence of steel casing in the bore holes. In one electromagnetic method the conductivity outside the casing can be measured if the source is a large loop on the surface and the sensor is inside the casing. For most of the methods, however, the metal casing will effectively short the source.

For dc methods there are some possibilities for surveys which use the casing itself, or insulated sections of it, as current or measuring electrodes. The current is connected to the casing at a point and the resulting potentials in the medium are governed by the conductivity and cross-section of the casing and the conductivity of the surroundings. There are two limiting cases for the potential distribution: If the casing is very thin and resistive, the field will be close to that of a point source; If the casing is thick and conductive (or perfectly conducting), it will be close to a line source.

Modeling of field data using the perfectly conducting filamental line source appears to show some disagreements in the far-field. It has been suggested that the current density in the pipe decreases with distance away from the actual source since the pipe is not a perfect conductor. At long distance, this deviation from the perfect line source may result in measurements that are more typical of a point source. If this hypothesis proves correct, then far-field (with respect to the source) data could be interpreted using point source solutions.

A simple half space potential field solution has been produced to test this hypothesis. The formulation of the half space case is done by using a whole space model and then applying the method of images to obtain the desired solution. The potential field is produced by a point source on the axis of an infinite pipe of finite conductivity (Figure 10a).

For this simple model, the borehole fluid, pipe, and adjacent rock are considered homogeneous with respective resistivities of ρ_1, ρ_2, and ρ_3. The region of the fluid lies within $r<r_1$, the the steel casing is in the region $r_1<r<r_2$, and the surrounding host rock is in the region $r>r_2$. The current source is located at the origin of the cylindrical coordinate system. Since this problem has symmetry about the polar axis, the appropriate equations are:

$$\nabla^2\Psi = C \ , \tag{1a}$$

$$\nabla^2\Psi = 0 \ , \tag{1b}$$

where Ψ is the potential and C is a constant. Equation 1a is the differential equation for the region containing the source (borehole fluid). The other expression (equation 1b) is for the regions excluding the source, i.e., the steel pipe and adjacent host.

For cylindrical coordinate system, the Laplacian of equation 1 can be written as:

$$\frac{1}{r}\frac{\partial}{\partial r}\left[r\frac{\partial\Psi}{\partial r}\right] + \frac{\partial^2\Psi}{\partial z^2} = C \ ,$$

$$\frac{1}{r}\frac{\partial}{\partial r}\left[r\frac{\partial\Psi}{\partial r}\right] + \frac{\partial^2\Psi}{\partial z^2} = 0 \ .$$

Taking the Hankel and Fourier transformations results in

$$-\left(\lambda^2 + \alpha^2\right)\tilde{\tilde{\Psi}} = \tilde{\tilde{C}} \ , \tag{2a}$$

$$-\left(\lambda^2 + \alpha^2\right)\tilde{\tilde{\Psi}} = 0 \ , \tag{2b}$$

where λ and α are the Hankel and Fourier transform variables, respectively and $\tilde{\tilde{\Psi}}$ is the twice transformed potential Ψ.

Equation 2a will yield the particular solution:

$$\Psi_p = \frac{2C}{\pi}\int_0^\infty K_0(\alpha r)\cos(\alpha z)d\alpha \ , \tag{3}$$

where $C=\frac{I\rho_1}{4\pi}$. The general solution of the homogeneous equation 2b is:

$$\Psi_i = \frac{2C}{\pi}\int_0^\infty \left[A_i(\alpha)K_0(\alpha r) + B_i(\alpha)I_0(\alpha r)\right]\cos(\alpha z)d\alpha \ . \qquad (4)$$

In region 1, $A_1(\alpha)$ must be zero since the modified Bessel function $K_0(x)\to\infty$ as $x\to 0$ and Ψ must be finite. Also, $B_3(\alpha)$ must be zero since the function $I_0(x)\to\infty$ as $x\to\infty$ and $\Psi\to 0$. The expression for the potential in region 1 is the sum of the particular solution from equation 3 and the homogeneous solution from equation 4 with $A_1(\alpha) = 0$. The three potential solutions at any field point (r,z) for the three regions are:

$$\Psi_1 = \frac{I\rho_1}{2\pi^2}\int_0^\infty \left[K_0(\alpha r)+B_1(\alpha)I_0(\alpha r)\right]\cos(\alpha z)d\alpha \ , \qquad (5a)$$

$$\Psi_2 = \frac{I\rho_1}{2\pi^2}\int_0^\infty \left[A_2(\alpha)K_0(\alpha r)+B_2(\alpha)I_1(\alpha r)\right]\cos(\alpha z)d\alpha \ , \qquad (5b)$$

$$\Psi_3 = \frac{I\rho_1}{2\pi^2}\int_0^\infty \left[A_3(\alpha)K_0(\alpha r)\right]\cos(\alpha z)d\alpha \ . \qquad (5c)$$

The constants B_1, A_2, B_2, and A_3 can be obtained by requiring the potentials and the normal current densities be continuous across the boundary surfaces. That is:

$$\Psi_1 = \Psi_2 \ , \qquad \frac{1}{\rho_1}\frac{\partial\Psi_1}{\partial r} = \frac{1}{\rho_2}\frac{\partial\Psi_2}{\partial r} \ , \qquad at \quad r = r_1 \ ,$$

and

$$\Psi_2 = \Psi_3 \ , \qquad \frac{1}{\rho_2}\frac{\partial\Psi_2}{\partial r} = \frac{1}{\rho_3}\frac{\partial\Psi_3}{\partial r} \ , \qquad at \quad r = r_2 \ .$$

Since only the potential outside of the well are of interest, the expressions for the potential Ψ_3 is only needed. Hence, A_3 needs to be solved by applying the boundary conditions. After much algebra, the expression for A_3 is obtained:

$$A_3(\alpha) = \left[\Gamma_1\Gamma_2+(1+\Delta_1)(1+\Delta_2)\right]^{-1} \ .$$

where:

$$\Gamma_1 = \alpha r_1 \left(\frac{\rho_1}{\rho_2} - 1 \right) I_0(\alpha r_1) I_1(\alpha r_1) \ ,$$

$$\Gamma_2 = \alpha r_2 \left(\frac{\rho_2}{\rho_3} - 1 \right) K_0(\alpha r_2) K_1(\alpha r_2) \ ,$$

$$\Delta_1 = \alpha r_1 \left(\frac{\rho_1}{\rho_2} - 1 \right) I_0(\alpha r_1) K_1(\alpha r_1) \ ,$$

$$\Delta_2 = \alpha r_2 \left(\frac{\rho_2}{\rho_3} - 1 \right) I_0(\alpha r_2) K_1(\alpha r_2) \ .$$

The following properties of Bessel functions were used:

$$\frac{\partial}{\partial x} I_0(x) = I_1(x) \ , \qquad \frac{\partial}{\partial x} K_0(x) = -K_1(x) \ ,$$

and

$$I_0(x) K_1(x) + I_1(x) K_0(x) = \frac{1}{x} \ .$$

The actual potential is obtained by numerical integration of expression 5c. The numerical integration was achieved by using a lag convolution algorithm developed by Anderson (1975) that evaluates the cosine transform. The potential routine was tested using a whole space model. The results showed that the error from the exact solution from using the single precision lag convolution to calculate the potential of equation 5b was approximately 0.001 %.

Figure 10b shows the set up for the half-space case. The major difference from the whole space is that the upper half space acts as a perfect insulator; hence no electrical current can flow across the surface (z=0). By imaging the subsurface across this boundary will result in a no current flow boundary at z=0. The vertical current contributions from the source and its image will be equal and opposite, thus cancelling each other. The radial components, having the same sign, will sum.

Figure 11a is a typical plot of the potentials for the cased-well, Ψ_{CW} and the half space, Ψ_{HS} in the radial direction. Near the source, the cased-well potential amplitude is smaller than that of the half space and falls off as $\ln r$ (line source). This is due to the current flowing in the conductive pipe and slowly "leaking" into the surrounding formation. As one moves radially away from the source, Ψ_{CW} will asymptotically approach Ψ_{HS} ($1/r$ fall off). Since the pipe is not a perfect conductor, the current in the pipe eventually is so minute that the pipe appears "finite" and at far-fields this will appear as a point source.

The vertical profile (Figure 11b) has a similar behavior. Near the pipe, the cased-well potential in the axial direction is nearly constant as it would be for a line source. At some distance, Ψ_{CW} becomes greater than Ψ_{HS}. Eventually, the potential of the cased-well asymptotes to the point source potential. But, the distance at which Ψ_{CW} asymptotes to Ψ_{HS} is farther from the source down the z-axis. From Figure 11, one may conclude that the semi-infinite pipe of finite conductance may be similar to a line source of a finite length.

With the above idea in mind, a contour plot of the percent difference (PD) between the half space and the cased-well potentials is given in Figure 12. The percent difference was calculated by the following formula:

$$PD = 100\% \cdot \left\{ \frac{\Psi_{HS} - \Psi_{CW}}{\Psi_{HS}} \right\} .$$

The two plots are spatially logarithmic so as to observe the character of the function over a large area. The upper plot is for field points above the source and the lower corresponds to points below the electrode. The resistivities of the borehole fluid and the surrounding rock were 100 Ωm. A resistivity of of 10^{-6} Ωm was used for the semi-infinite pipe. The depth of the current source was $100m$ and located on the z-axis.

Along the radial direction for z near the source ($\sim 100m$), $\Psi_{HS} \gg \Psi_{CW}$ which produces a percent difference near 100%. As one moves away, $\Psi_{CW} \rightarrow \Psi_{HS}$ and the percent difference approaches zero. In the downward axial direction, the percent difference begins near 100% decreases and reaches a negative minimum near 1 km below the source. Notice that the $PD < -100\%$ in this area. Near this 1 km depth, $\Psi_{CW} > \Psi_{HS}$ and $\Psi_{CW}, \Psi_{HS} \ll 1$ (also see Figure 11b). Since Ψ_{HS} is very small, the percent difference, being normalized by Ψ_{HS}, will be very large even though the values are small. As $\Psi_{CW} \rightarrow \Psi_{HS}$, the percent difference goes toward zero. The upper plot is similar to the lower one for similar locations away from the source.

It appears from the preliminary studies that one must be very far from the source in order to use the point source approximation for the solution. But, the data seem to indicate that a finite line source may be useful to approximate the potential. A problem encountered using this method is to choose a length for the line source. A length must be chosen so that the line source potential will respond like an actual pipe. The potential of the line source must asymptote to the half space solution at the far-fields. The distance which this occurs varies depending on the resistivities of the materials involved and on the thickness of the pipe.

Further studies are being conducted to compare the potentials of the semi-infinite pipe to a semi-infinite and finite length line source. From the comparisons, it is hoped that an "effective" length of the semi-infinite pipe can be determined so that the line source approximation can be used effectively. The current density in the surrounding medium is being calculated so as to obtain an understanding of the current pattern from a highly conductive pipe in a half space. Also, a solution for the potential field from a finite length of pipe in a layered half space, or for insulated segments of pipe, should be obtained for applications in an

actual field experiment.

In experiments being designed for mapping and monitoring in the vicinity of waste repositories it probably will be necessary to use non-metallic casing. Metal segments can easily be inserted as electrodes and the magnetic dipole electromagnetic methods would see no casing effect whatsoever.

C. Electromagnetic Methods

Electromagnetic methods have been used traditionally to locate conductivity inhomogeneities from surface transmitter-receiver configurations. Recently they have been used successfully to map subsurface conductivity in situations where the earth can be modelled with horizontal layers. Em has great advantages over dc resistivity in these situations since the sounding can be carried out with small transmitter-receiver separations (zero in the limit when the receiver is located within a horizontal loop transmitter) by varying the frequency or measuring the transient field after current in the transmitter is turned off. We have used such systems with success in geothermal and petroleum exploration (Wilt et al., 1983 and 1984).

A new and promising application is in subsurface or subsurface to surface methods. We have developed numerical methods to deal with the following three configurations that would be useful in subsurface mapping and, in particular, in the detection of fracture zones.

i) Surface to bore hole. In this configuration the transmitter is a horizontal loop on the surface coaxial with a bore hole, and the receiver (only vertical component of the field so far) is located in the hole. Results (Kennedy, 1984) show that :

a) The configuration has greater sensitivity to conductivity structure beyond the hole than surface or conventional well log methods.

b) The conductivity can be sensed through casing.

c) In layered media the currents (for any magnetic dipole source) flow parallel to layer boundaries so only horizontal conductivity is sensed. These measurements are complementary to dc resistivity since the latter senses both horizontal and vertical conductivity.

ii) Subsurface magnetic dipole source. We have developed the general solution for magnetic dipoles within a layered medium and have applied the solution to the general induction logging problem in an inclined or deviated bore hole (Kennedy et al., 1986). The program is well suited to an analysis of cross hole em measurements in layered media.

We have also developed the solution for scattered fields on the surface from a subsurface planar conductor (Zhou and Becker, 1986) in the presence of a subsurface magnetic dipole. This study clearly showed that planar conductors representing fracture zones could be detected with such an array. This program is also easily modified for cross hole or in-hole reflectance studies of such features. These studies assume uncased or plastic-cased holes.

iii) Subsurface vertical electric dipole source. This is one of the most promising sources for subsurface em since there are no magnetic fields on the surface if the source is located in a horizontally layered medium. Inhomogeneities, such as the planar conductors, do produce anomalous magnetic fields on the surface so that this is an ideal configuration for location and detection of fracture zones. Preliminary results show anomalies for sheet-like conductors to be as distinct for the vertical electric dipole source as for the magnetic dipole source. Further, the em results seem more diagnostic of the parameters of the fracture than the dc results described by Beasley and Ward (1986). As the frequency is increased this solution extends to the use of radar methods. At low frequencies grounded electrodes are necessary. Thus

an uncased hole or plastic-cased hole fitted with metal electrodes would be required.

Examples of these results over a thin sheet conductor in a conductive half space are given in Figures 14 to 18. The model shown in Figure 13 is a rectangular thin plate of conductance τ. Its upper edge is horizontal and at a depth H beneath the surface. The strike length is L_a and the dip length L_b; the dip is β. The plate is located in a half space of conductivity σ_2 overlain by a layer of conductivity σ_1 and thickness D. The source, either a vertical magnetic dipole, VMD, or a vertical electric dipole, VED, can be located anywhere and the magnetic and electric fields are calculated anywhere in the medium (except very close to the plate). The solutions are obtained in the frequency domain and the transient fields are calculated by Fourier transformation.

In these examples, fields on the surface have been calculated for a model of a vertical plate with a conductance of one siemen lodged in a half space of 100 ohm m with no overburden layer. The strike length is 100 m, the dip length 60 m, and the depth to the top edge is 30 m. The dipole source is located at a depth of 100 m and is 100 m to the left of the conducting plate.

In Figures 14, 15 and 16 the secondary magnetic fields in the x, y, and z directions respectively for the VED source are plotted for a frequency of 1000 Hz. The secondary magnetic fields in the x,y, and z direction from a VMD source are shown in Figure 17 and 18. There are several features of these :

a) There is no primary field from the VED so the secondary field is the only field to be measured. The secondary field from the VMD would have to be measured in the presence of the primary field, the usual difficulty of most surface em systems.

b) The anomalies from the VED are more complex than those from the VMD. This might suggest greater information about the plate, but this has not been studied.

c) The anomalies are surprisingly distinct for such a low conductance and the method shows promise for detecting much lower conductances with suitable frequencies and favorable host rock resistivities.

d) The ultimate comparison will depend on the practical moments that could be achieved with in hole VMD or VED transmitters. The results presented here are for unit moments.

e) As frequency increases the solutions for the VED go toward the radar solution. The technique used for this analysis is ideally suited for investigating the heretofore unstudied region between the diffusion (low frequency) regime and the radar (high frequency) regime.

The planar conductor in these illustrations was modelled using an algorithm developed by Weidelt (1981) for surface magnetic dipole sources and modified by us for arbitrary sources in the subsurface. The calculations can be done for either frequency or time domain sources. We also have two more general algorithms for surface sources over arbitrary 2-D models (Lee and Morrison, 1985) or over three-dimensional confined conductors (Lee et al., 1981). These programs must be generalized to handle subsurface sources.

Much research needs to be done to determine which of these configurations is best suited to the needs of characterizing and monitoring the repository site. It is likely that a combination of dc electrical and em methods will prove best for detecting fracture zones from a bore hole or excavation while others will be best for monitoring the site before, during, and after waste emplacement. The basic numerical

programs are available but they would have to be be modified to deal with the particular features of the waste repository studies.

D. Radar Methods

The use of very high frequency em methods may be very useful in mapping in the vicinity of repositories situated in highly resistive rock.

Ground-penetrating Radar (GPR) is a relatively new geophysical technique. It consists of emitting a high-frequency pulse of electromagnetic energy and recording the returned echoes -- as in ordinary radar, sonar, and vertical incidence seismic profiling. The time delay is determined by the speed of light in the medium and the returned signal strength is determined by the contrast in the speed of light in the two media, attenuation between source and receiver antenna, and geometrical spacing (Ulriksen, 1982). The Canadian nuclear waste repository program has successfully used GPR to map fractures in three dimensions in a granitic intrusion (Holloway, 1985).

Attenuation is chiefly determined by the resistivity of the material and the frequency used, the attenuation increasing with decreasing resistivity and increasing frequency. In a dry, resistive material such a tuff granite or salt, the attenuation will be low and penetration depths of tens of meters can be expected (Olhoeft, 1985).

The speed of light in most geological materials is determined by the dielectric constant of the material, which in turn is determined largely by the water content. In a homogeneous material, such as thick tuff or salt beds, the major discontinuities in light velocity will be caused by (fluid-filled) fractures.

GPR thus provides a rapid, reliable means of locating water, clay and fractures within the repository as a preliminary assessment technique and to monitor fracturing as mining progresses.

4. Monitoring Changes in Subsurface Conductivity

All of the electrical and electromagnetic methods discussed above for mapping the conductivity distribution can, in principle, be used to monitor changes in the conductivity. In practice, there will be constraints imposed either by site requirements, geological features, or nature of contaminating noise that will probably eliminate certain of the methods. Radar for example will have a relatively short range, ≈ 100 m, and requires considerable power and instrumentation : it is unlikely that it would be either permitted or convenient to use within the repository for long term monitoring, post emplacement. DC resistivity on the other hand is known to be very sensitive to large volume changes in conductivity and we have seen from our preliminary modelling that all the electrodes can be completely outside the repository. EM models are sensitive to both volume changes in conductivity and to individual fracture zones. For one configuration, the VED , the method is only sensitive to the inhomogeneities in a layered section.

For all these methods the fundamental question of signal to noise will dictate the final accuracy with which time changes can be monitored. Source moment and signal averaging have been the only two parameters that can be increased to improve signal to noise. Recently we have completed field studies (Nichols et al., 1985) of a technique to use remote station noise cancellation to dramatically improve signal to noise. The concept is very simple. The natural electromagnetic field noise in which signals from dc or em methods are to be detected is remarkably coherent for many kilometers over the surface. Thus the fields at a remote site can be used to predict field at a local measurement site and the noise can be subtracted from the data. In a magnetic proppant injection experiment at a test site at Mounds Oklahoma we achieved noise reductions (of 60 db) in magnetic field with a remote site 1.5 km away.

The impact of this is greatest on subsurface source configurations where it may be difficult to emplace transmitters with adequate moment. For a magnetic dipole source the moment is the product of the number of turns, the area, and the current (and the effective permeability of the core if the coil is wound solonoidally). To obtain adequate signal with reasonable stacking this source must yield secondary fields at least equal to the natural noise field. With 60 db of noise reduction it is clear that moments or signal levels previously thought to be unachievable are now possible. This obviously will have a major impact on the application of these methods.

5. References

Archie, G.E., 1942; The Electrical Resistivity Log as an Aid in Determining some Reservoir Characteristics. AIME Transaction, vol.146, 54-62

Archie, G.E., 1947; Electrical Resistivity as an Aid in Core-analysis Interpretation. Am. Assoc. Petroleum Geologists Bull., vol. 31, no. 2, 350-366

Arps, J.J., 1953; The Effects of Temperature on the Density and Electrical Resistivity of Sodium Chloride Solutions. J. Petrol. Tech., vol. 6, 17-20

Asch,T., Wilt, M., Tsang, C.F., and Morrison. H.F., 1986; Monitoring Subsurface Contaminants with Borehole-to-Surface Resistivity Measurements. Earth Sciences Division Newsletter, vol. 9, no. 1, Lawrence Berkeley Laboratory, University of California, Berkeley

Beasley, C.W. and Ward, S.H., 1986; Three-dimensional Mise-a-la-masse Modeling Applied to Mapping Fracture Zones. Geophysics, vol. 51, no. 1, 98-113

Beyer, H., 1977c; Telluric and DC Resistivity Techniques Applied to the Geophysical Investigation of Basin and Range Geothermal Systems, Part III : The Analysis of Data from Grass Valley, Nevada. LBL-6325-3/3, Lawrence Berkeley Laboratory, University of California, Berkeley

Brace, W.F., Orange, A.S., and Madden, T.R., 1965; The Effect of Pressure on the Electrical Resistivity of Water-saturated Crystalline Rocks. J.G.R., vol. 70, no. 22, 5669-5678

Brace, W.F. and Orange, A.S., 1968a; Electrical Resistivity Changes in Saturated Rocks during Fracture and Frictional Sliding. J.G.R., vol. 73, no .4, 1433-1445

Brace, W.F. and Orange, A.S., 1968b; Further Studies of the Effects of Pressure on Electrical Resistivity of Rocks. J.G.R., vol. 73, no. 16,

5407-5420

Campbell, D.L., 1977; Short Note: Model for Estimating Electrical Macroanisotropy Coefficient of Aquifers with Horizontal and Vertical Fractures. Geophysics, vol. 42, no. 1, 114-117

Daniels, J.J., 1977; Three-dimensional Resistivity and Induced Polarization Modeling using Buried Electrodes. Geophysics, vol. 42, no. 5, 1006-1019

Daniels, J.J., 1978; Interpretation of Buried Electrode Resistivity Data using a Layered Earth Model. Geophysics, vol. 43, no. 5, 988-1001

Daniels, J.J., 1983; Hole-to-Surface Resistivity Measurements. Geophysics, vol. 48, no. 1, 87-97

Daniels, J.J. and Dyck, A.V., 1984; Borehole Resistivity and Electromagnetic Methods Applied to Mineral Exploration. Transactions on Geoscience and Remote Sensing, IEEE, GE-22, 80-87

Dey, A. and Morrison, H.F., 1976; Resistivity Modeling for Arbitrarily Two-dimensional Structures, Part I: Theoretical Formulation. LBL-5223, Lawrence Berkeley Laboratory, University of California, Berkeley

Dey, A., 1976; Resistivity Modeling for Arbitrarily Two-dimensional Structures, Part II : User's Guide to the FORTRAN Algorithm RESIS 2D. LBL-5283, Lawrence Berkeley Laboratory, University of California, Berkeley

Dey, A. and Morrison, H.F., 1979; Resistivity Modeling for Arbitrarily Shaped Three-dimensional Structures. Geophysics, vol. 44, no. 4

Dobecki, T.L., 1980; Borehole Resistivity Curves near Spheroidal Masses. Geophysics, vol. 45, no. 10, 1513-1522

Glanville, C.R., 1959; Laboratory Study Indicates Significant Effect of Pressure on Resistivity of Reservoir Rock. J. Petrol. Tech., vol. 11, no. 4, 20-26

Grant, F.S. and West, G.F., 1965; Interpretation Theory in Applied Geophysics. Mc Graw Hill, New York

Greenberg, R.J. and Brace, W.F., 1969; Archie's Law for Rocks Modeled by Simple Network. J.G.R., vol. 74, no. 8, 2099-2102

Hill, D.G., 1972; A Laboratory Investigation of Electrical Anisotropy in Precambrian Rocks. Geophysics, vol. 37, 1022-1038

Hoeing, Alan, 1978/1979; Electric Conductivities of a Cracked Solid. Pure and Applied Geophysics, vol. 117, 690-710

Ibrahim, A.W. and Keller, G.V., 1981; Seismic Velocities and Electrical Resistivity of Recent Volcanics and their Dependence on Porosity, Temperature, and Water Saturation. Geophysics, vol. 46, 1415-1422

Keller, G.V. and Frischknecht, F.C., 1966; Electrical Methods in Geophysical Prospecting. Pergamon Press, New York

Keller, G.V., 1966; Dipole Method for Deep Resistivity Studies. Geophysics, vol. 31, no. 6, 1105-1122

Keller, G.V., Furgerson, R., Lee, C.Y. Harthill, N. and Jacobson, J.J., 1975; The Dipole Mapping Method. Geophysics, vol. 40, no. 3, 451-472

Kennedy, W.D., Corry, S.M., All. S.P. and Morrison H.F., 1986; Induction Log Response in Deviated Boreholes. SPWLA, 27th Annual Logging Symposium, June 9-13, 1986, Atlanta

Lee, K.H., Pridmore, D. F. and Morrison, H.F., 1981; A Hybrid Three-Dimensional Electromagnetic Modeling Scheme. Geophysics, vol. 46, no. 5, 796-805.

Lee, K.H. and Morrison, H.F., 1985; A Numerical Solution for the Electromagnetic Scattering by a Two-Dimensional Inhomogeneity. Geophysics, vol. 50, no. 3, 466-472.

Leonard-Mayer, P.J., 1983; Development of a Surface Resistivity Method for Jointed Formations: Field Study. Geophysics Abstracts, 125-127

Long, J.C.S. and Witherspoon, P.A., 1965; The Relationship of the Degree of Interconnection to Permeability in Fracture Networks. Journal of Geophysical Research, vol. 90, no. B4, 3087-3098

Lytle, T.J., 1982; Resistivity and Induced Polarization : Probing in the Vicinity of a Spherical Anomaly. Transactions on Geoscience and Remote Sensing, IEEE, GE-20, no. 4, 493-499

Lytle, R.J. and Hanson, J.M., 1983; Electrode Configuration Influence on Resistivity Measurements about a Spherical Anomaly. Geophysics, vol. 48, no. 8, 1113-1119

Madden, T.R., 1976; Random Network and Mixing Laws. Geophysics, vol. 451, 1104-1125

Morrison, H.F., Lee, Ki Ha and Kennedy, W.D., 1984; Low Frequency Electromagnetic Logging. SEG 54th Annual International Meeting, Dec. 2-6, 1984, Atlanta

Olhoeft, G.R., 1981; Electrical Properties of Granite with Implications for the Lower Crust.

Sasaki, Y., 1982; Automatic Interpretation of Induced Polarization Data over Two-dimensional Structures. Mem. Faculty Eng., Kyuschu University, vol. 42, no. 1, 59-74

Shankland, T.J. and Waff, H.S., 1974a; Conductivity in Fluid-bearing Rocks. J.G.R., vol. 79, no. 32, 863-4868

Tseleentis, Gerasimos-Akis, 1985; A Study of the Hydrogeophysical Properties of Fissured Aquifers using a Double Porosity Model. J. of Hydrology, vol. 78, 331-344

Van Nostrand, R.G. and Cook, K.L., 1966; Interpretation of Resistivity Data. U.S. Geol. Survey Prof. Paper 499

Wilt, M.J., Pruess, K., Bodvarsson, G.S. and Goldstein, N.E., 1983; Geothermal Injection Monitoring with dc Resistivity Methods. Geothermal Research Council, Trans., vol. 7, Oct. 1983, 477-482

Wilt, M.J., Goldstein, N.E., Stark, M. Haught, J.R. and Morrison, H.F., 1983; Experience with the EM-60 Electromagnetic System for Geothermal Exploration in Nevada. Geophysics, vol. 48, no. 8, 1090-1101

Wilt, M.J., Goldstein, N.E. and Morrison, H.F., 1984; An Electromagnetic Sounding Survey in the Boylston- Yakima Area, Washington. Final Report to Shell Development Co., LBL Report, Jan. 1984

Wilt, M.J. and Tsang, C.F., 1985; Monitoring of Subsurface Contaminants with Borehole/Surface Resistivity Measurements. Presented at the 2nd National Conf. and Expos. on Surface and Borehole Geophysical Methods in Ground Water Investigation, NWWA, Ft. Worth, TX, Feb. 12-14, 1985, LBL Report no. LBL-19106

Yang, F.W. and Ward, S.H., 1985a; Single-borehole and Cross-borehole Resistivity Anomalies of Thin Ellipsoids and Spheroids. Geophysics, vol. 50, no. 4, 637-655

Yang, F.W. and Ward, S.H., 1985b; On Sensitivity of Surface-to-borehole Resistivity Measurements to the Attitude and the Depth to Center of a Three-dimensional Spheroid. Geophysics, vol. 50, no. 7, 1173-1178

Zhou, Q. and Becker, A., 1985; Distortion of Electromagnetic Waves by Geological Structure. Interim Report Engineering Geoscience, Contract # LLNL-7174105, Submitted to LLNL Dec. 1985

Figure 7d: Percent differences referenced to results from shallowest dipole (surface to 150 m)

Figure 7e: Percent differences referenced to dipole at 600-750 m depth

Figure 8a: Idealized repository model with two near surface conductive inhomogeneities

Figure 8b: Dipole-dipole pseudo-section over the model shown in Figure 8a

Figure 9a: Idealized repository model of Figure 8a with current electrodes in a hole passing through the repository

Figure 9b: Percent differences in apparent resistivity referenced to uniform half-space

Figure 9c: Percent differences in apparent resistivity referenced to results obtained with the source electrode within the repository

Figure 10: Cylindrical coordinates, electrical parameters and notation for a point source of current, I, in the bore of an infinite cylindrical casing in : a) a conductive whole space, and b) a half-space

Figure 11: Potential of a unit current source in a half-space and in a cased well as a function of: a) radial distance from the source, and b) z axis distance from source at a radial distance of one meter

Figure 12: Contour plot of the difference potential between a point source in a half-space and a point source in the cased hole as a percent of the half-space potential

Figure 13: Model parameters for a dipole source located within a two-layer earth in the presence of a thin conductive sheet

DEPENDENCE OF LONGITUDINAL CONDUCTIVITY ON FRACTURE POROSITY.

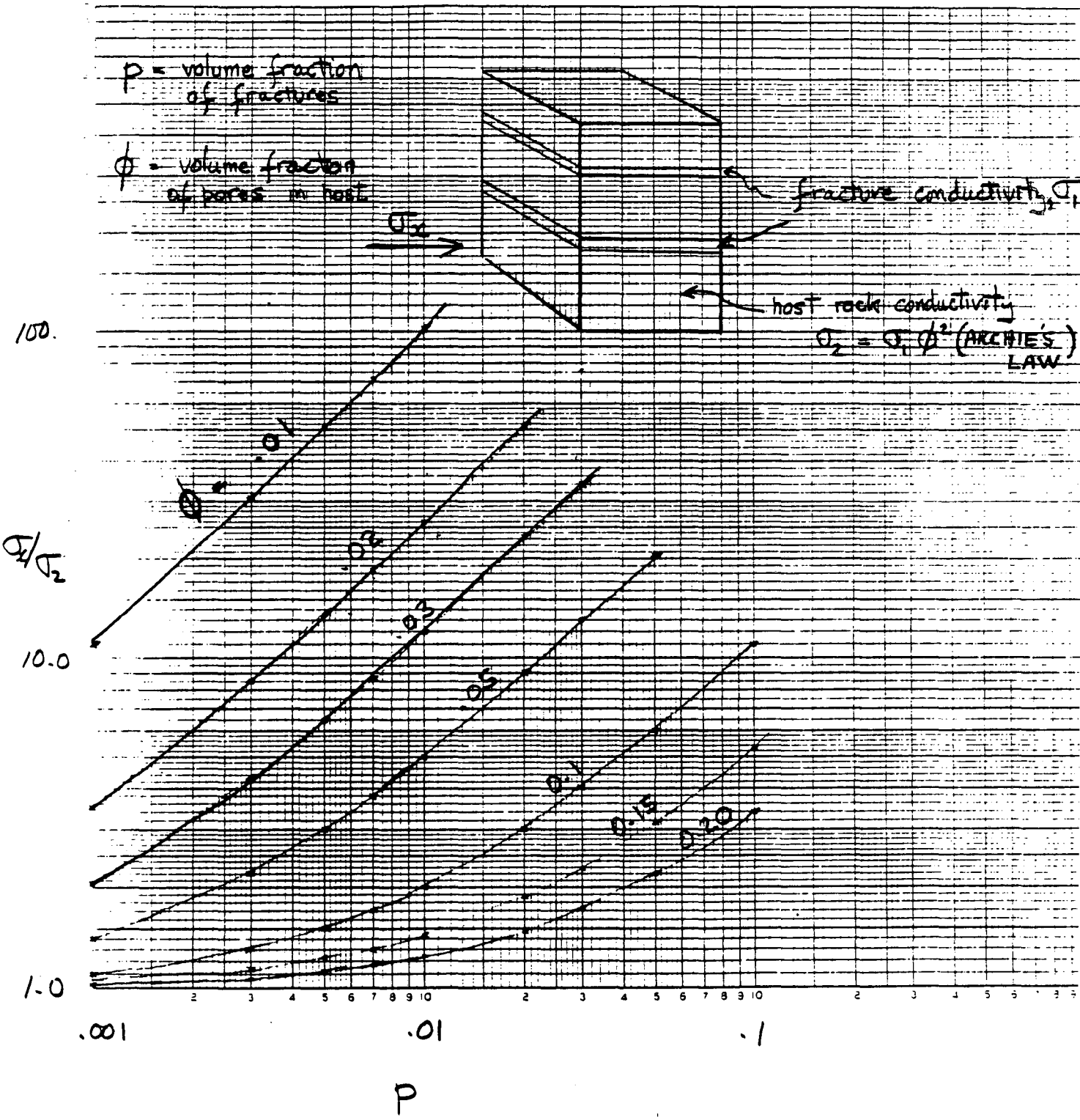

Figure 1

EFFECT OF FRACTRURE CLOSURE

ON THE RESISTIVITY OF GRANITE

(AFTER BRACE AND ORANGE, 1968)

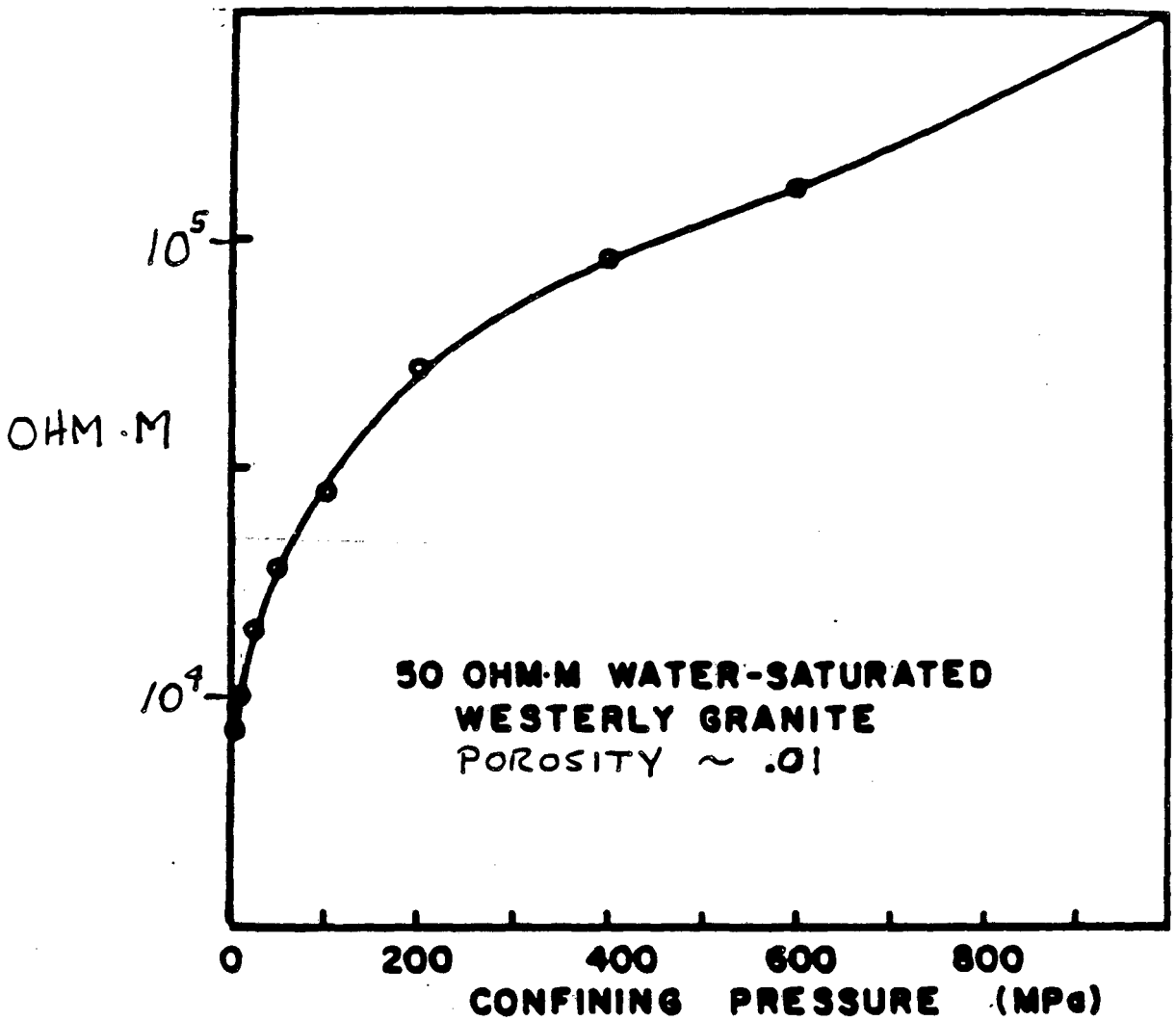

Figure 2

NUCLEAR STORAGE MODELLING: APPARENT RESISTIVITY DATA
DIPOLE-DIPOLE SURFACE SURVEY
RES52D: NUCLEAR ZONE 3 TIMES SURROUNDING RESISTIVITY

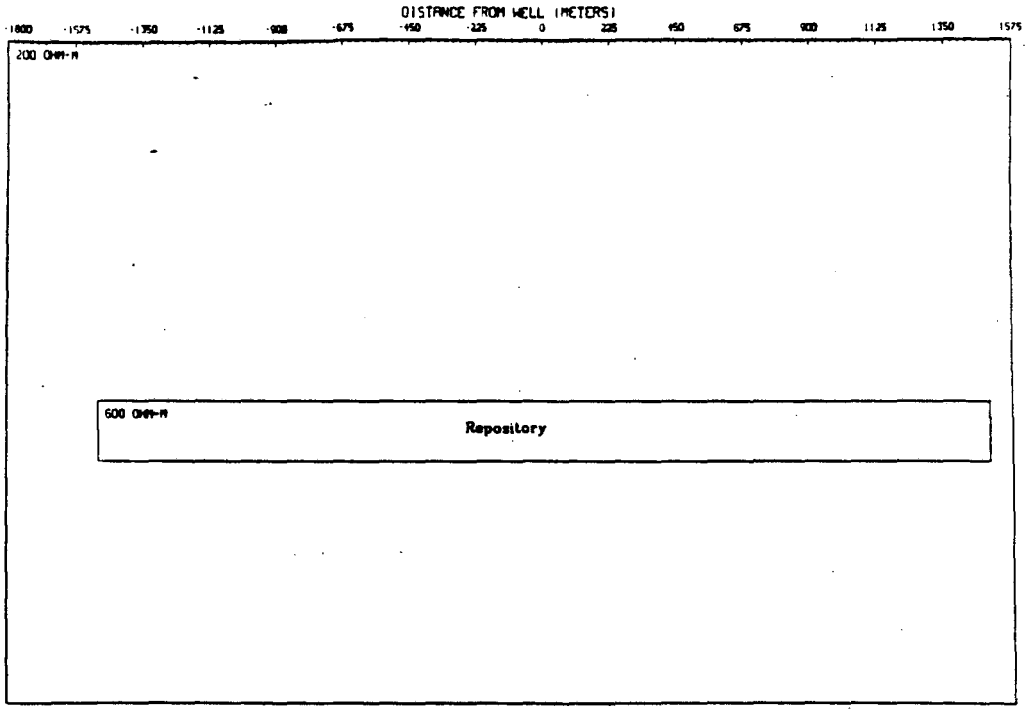

Figure 3

NUCLEAR STORAGE MODELLING: APPARENT RESISTIVITY DATA
DIPOLE-DIPOLE SURFACE SURVEY
RES52D: NUCLEAR ZONE 3 TIMES SURROUNDING RESISTIVITY

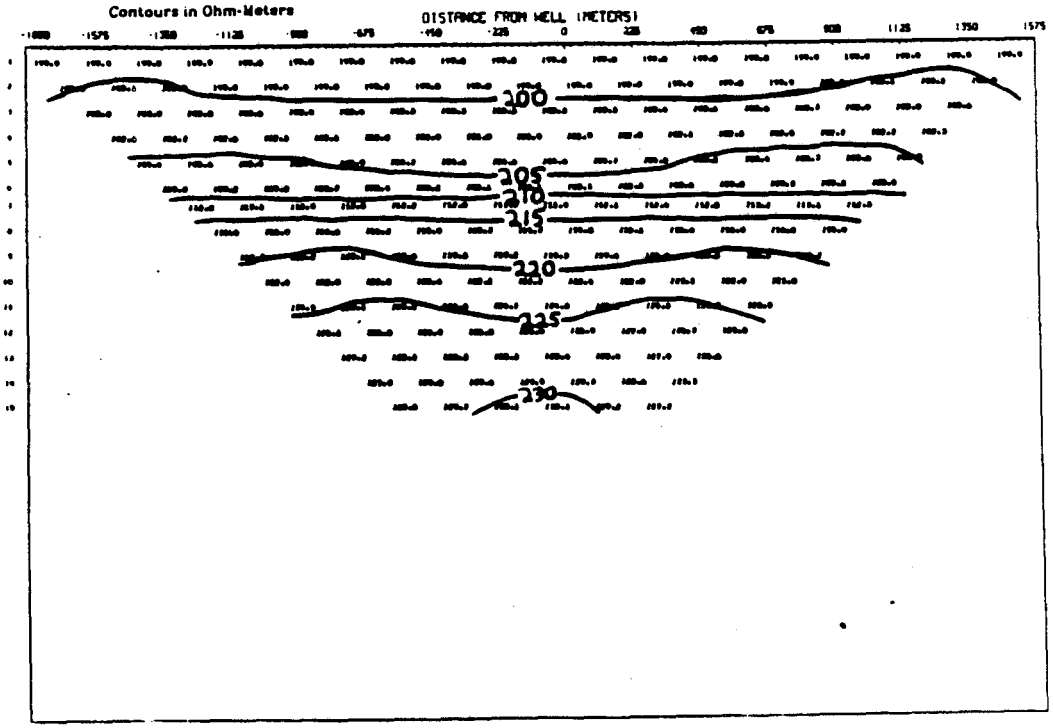

Figure 4a

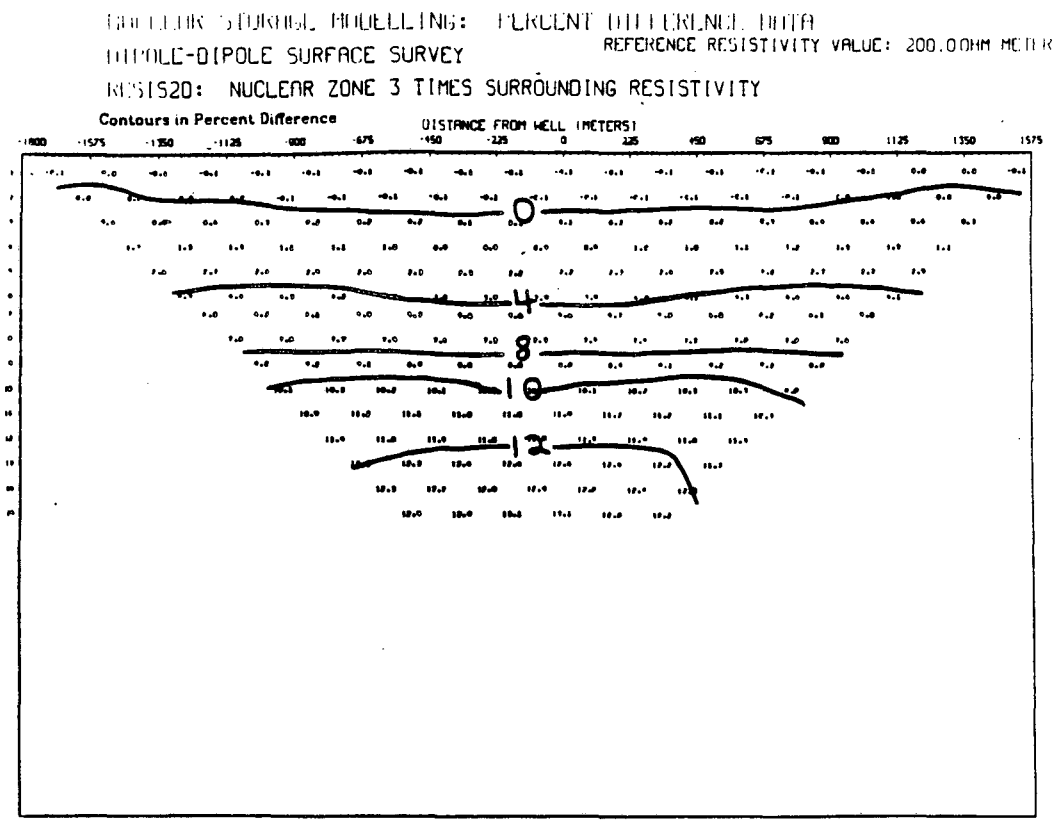

Figure 4b

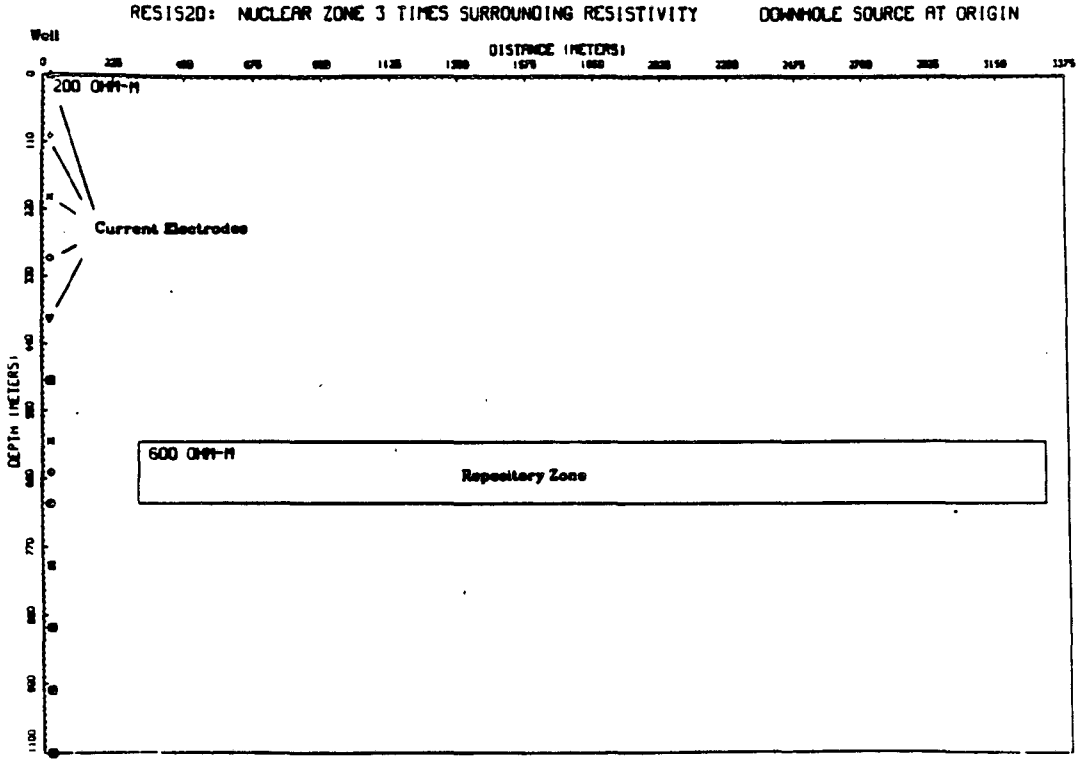

Figure 5a

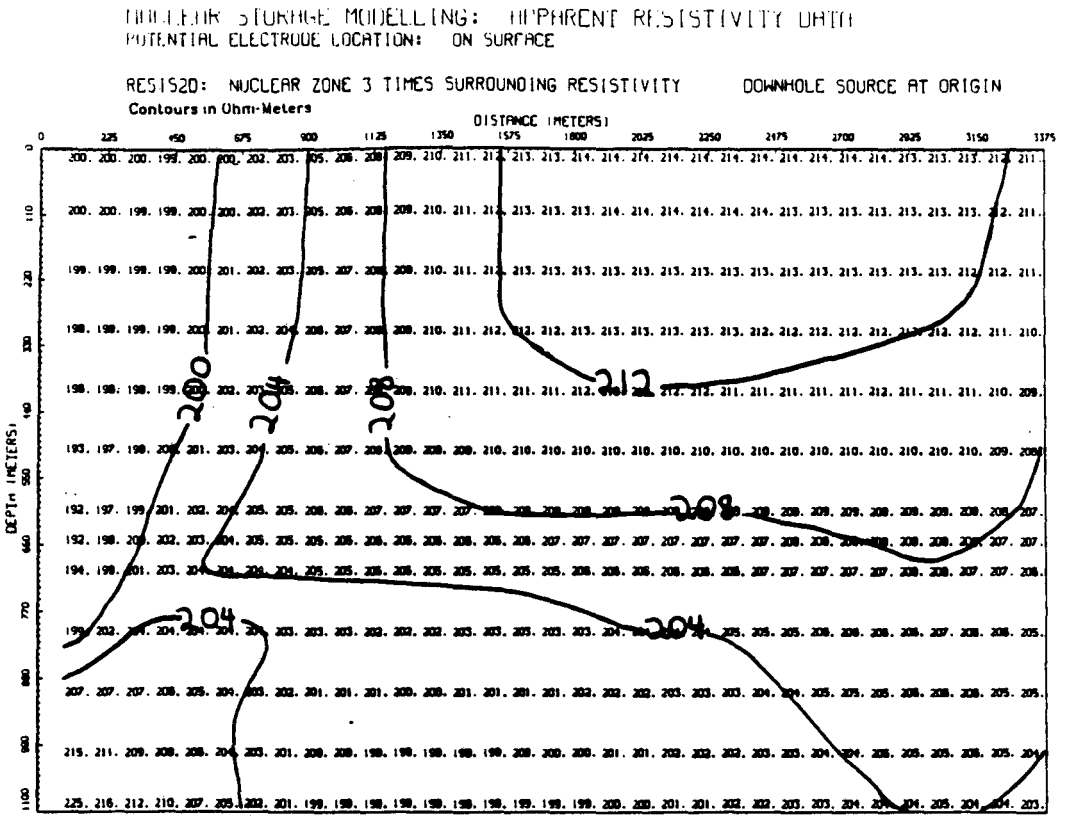

Figure 5b

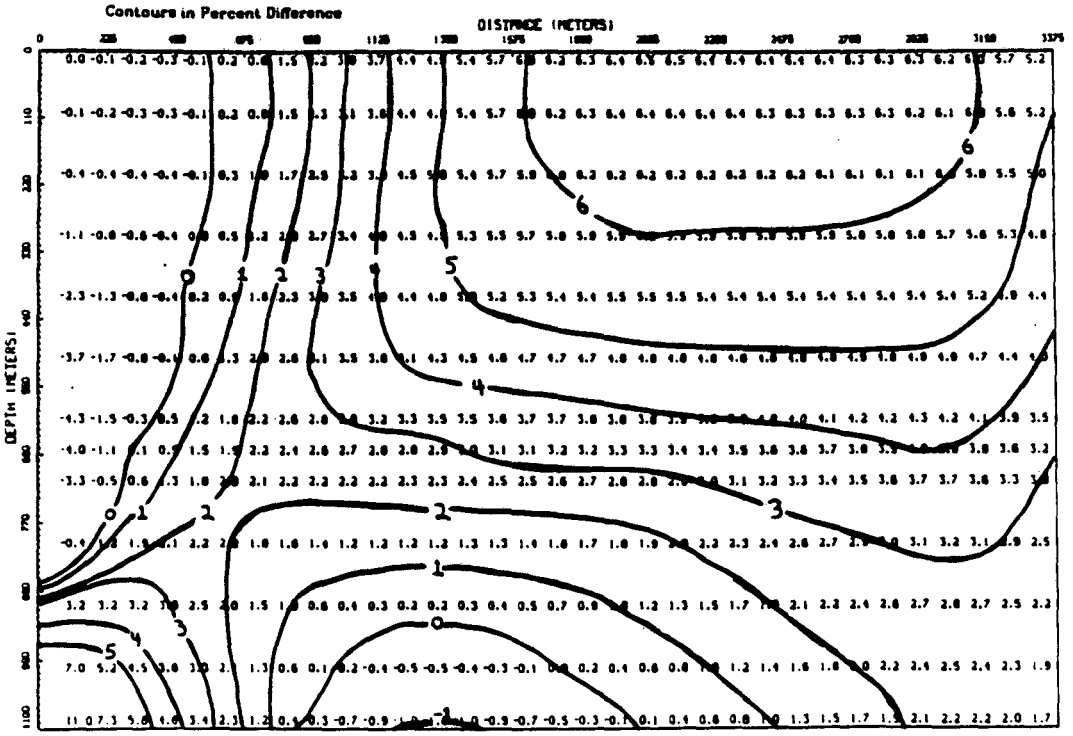

Figure 5c.

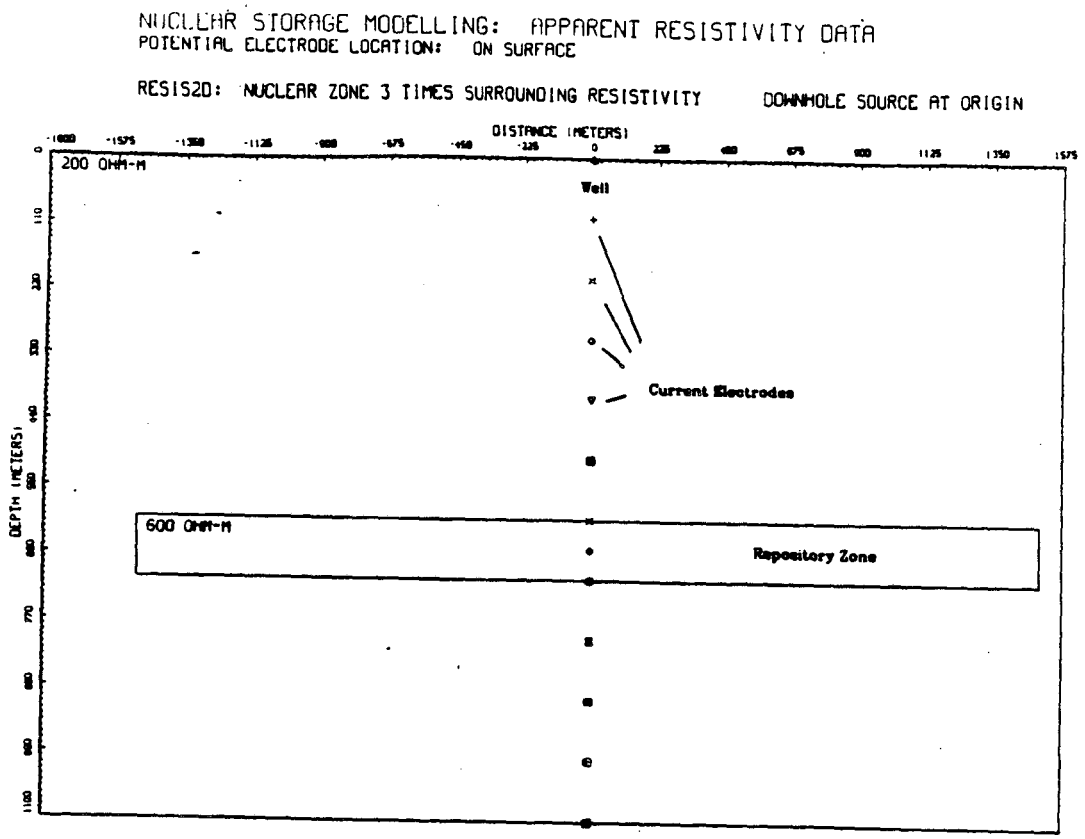

Figure 6a

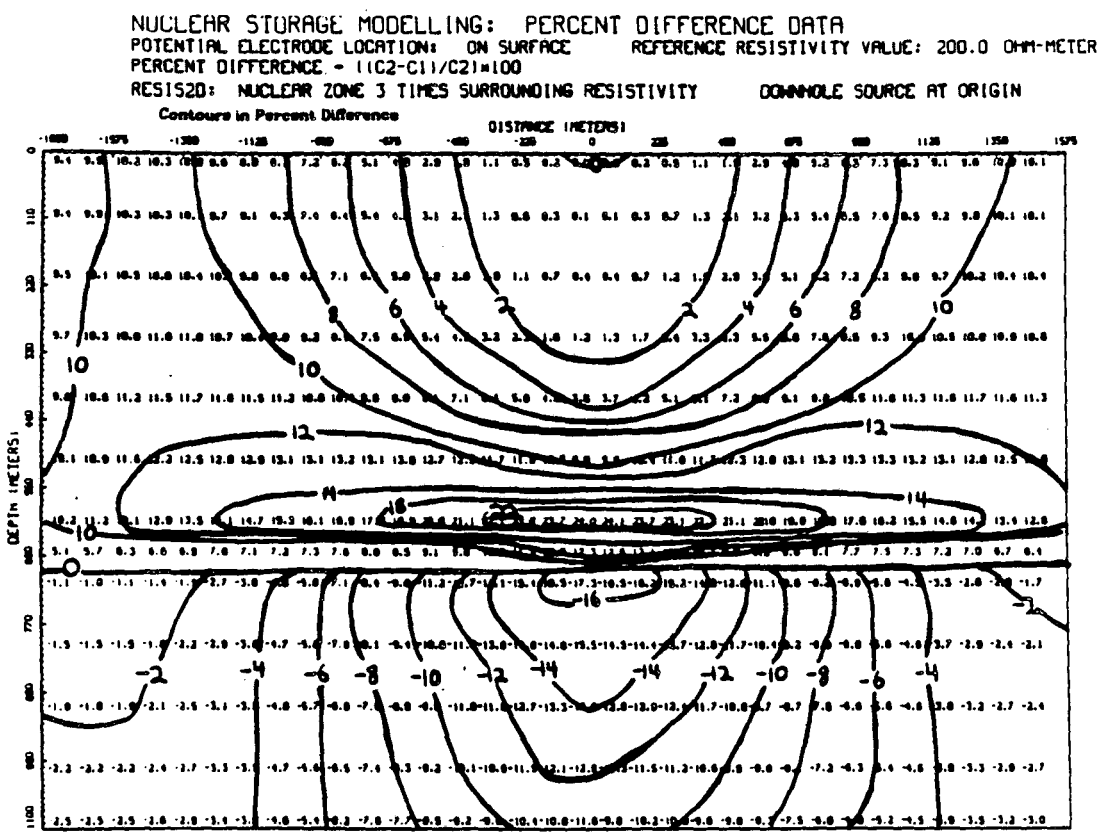

Figure 6b

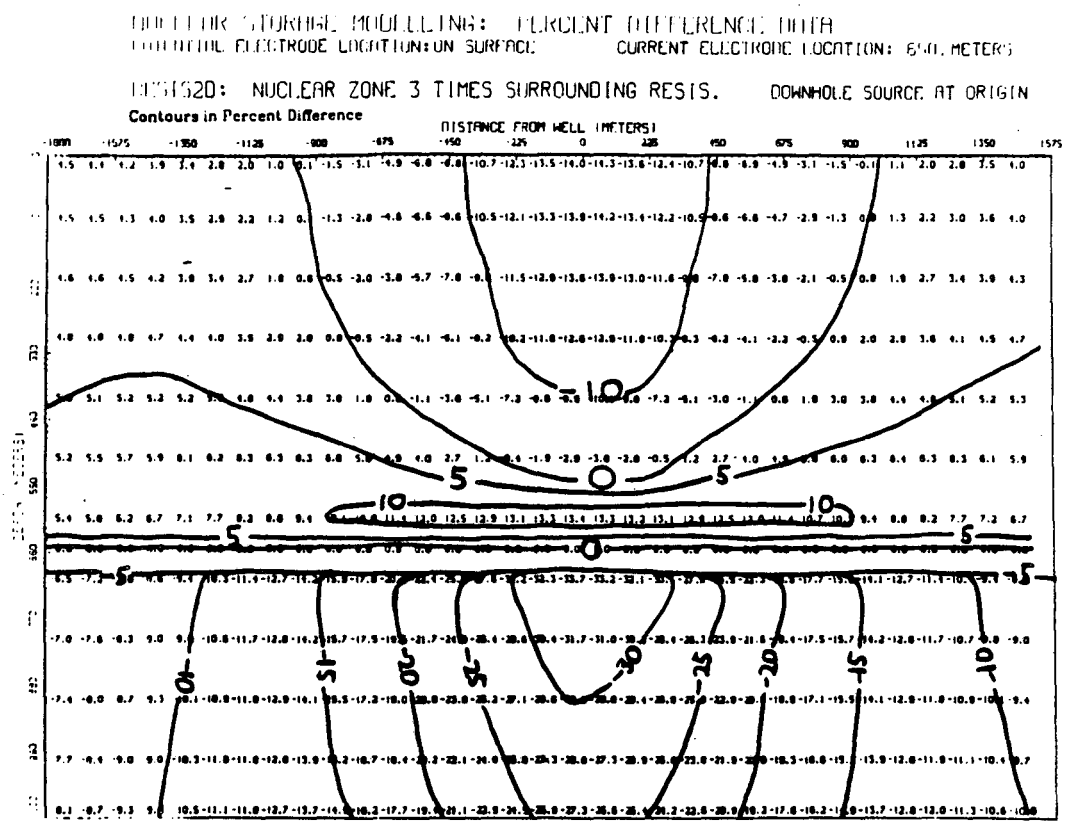

Figure 6c

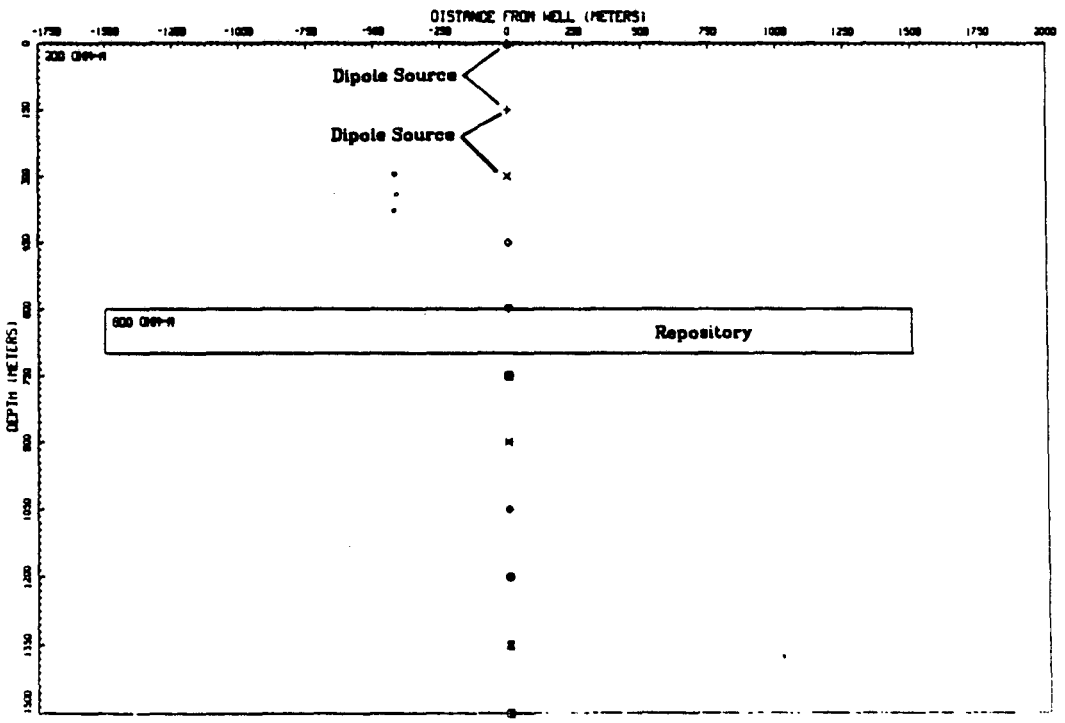

Figure 7a

NUCLEAR STORAGE MODELLING: APPARENT RESISTIVITY DATA
POTENTIAL ELECTRODE LOCATION:ON SURFACE

RESIS2D: DOWNHOLE DIPOLE-DIPOLE; SURFACE GRADIENT DOWNHOLE SOURCE AT ORIGIN

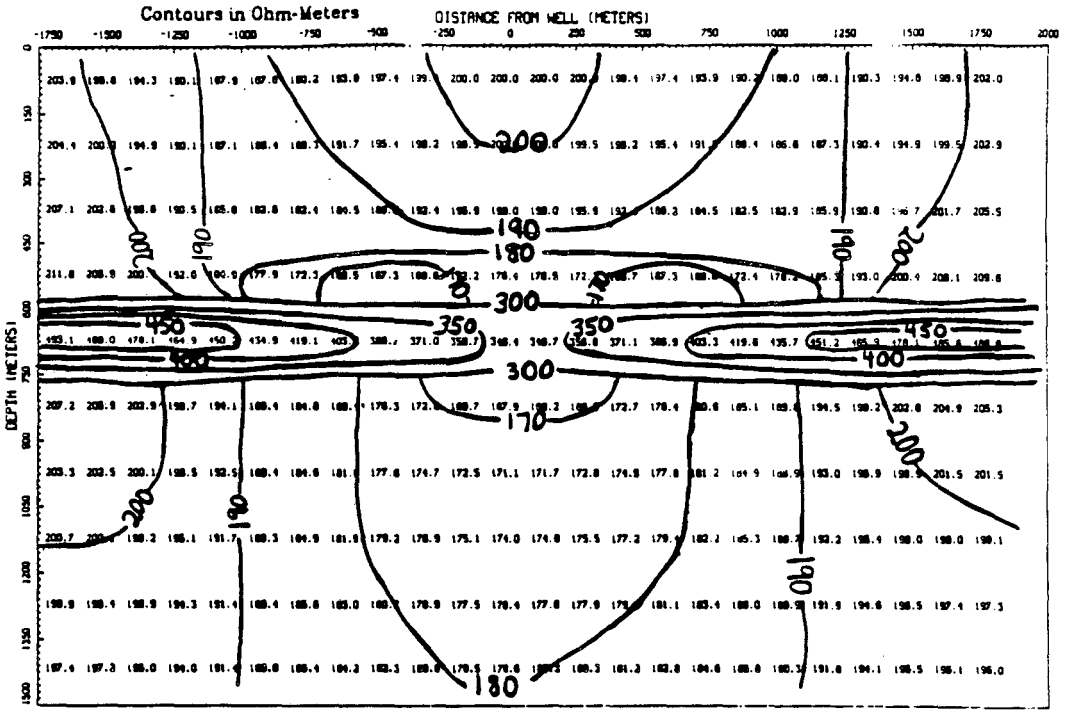

Figure 7b

NUCLEAR STORAGE MODELLING: PERCENT DIFFERENCE DATA
POTENTIAL ELECTRODE LOCATION:ON SURFACE REFERENCE RESISTIVITY VALUE: 200.0 OHM-METER

RESIS2D: DOWNHOLE DIPOLE-DIPOLE; SURFACE GRADIENT DOWNHOLE SOURCE AT ORIGIN

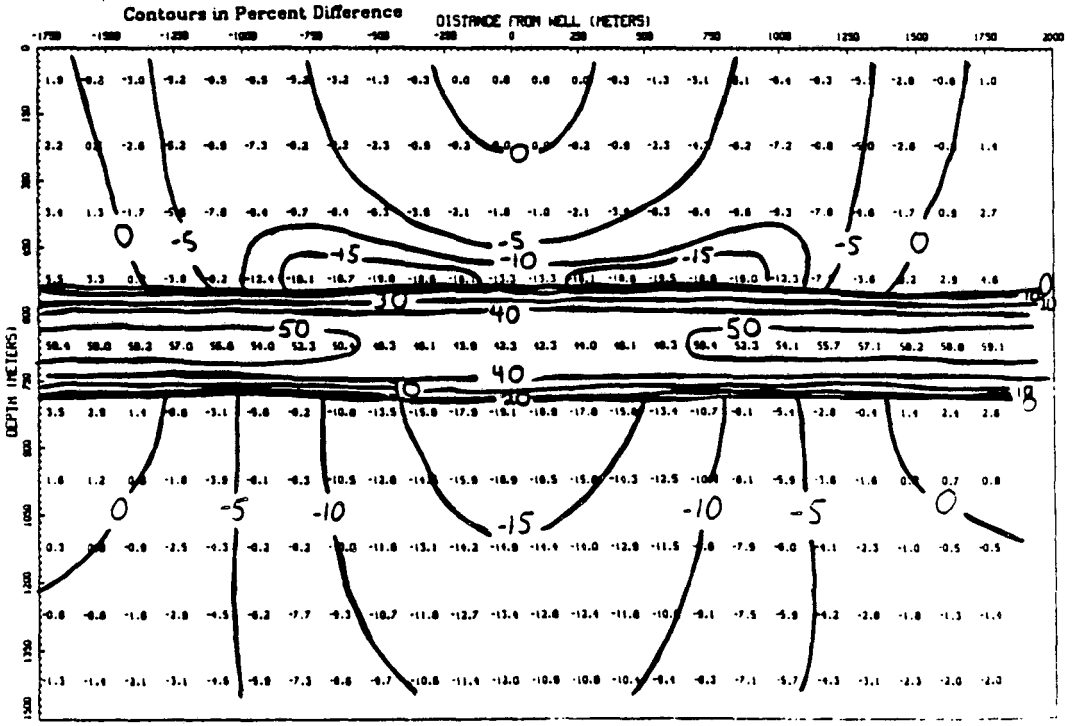

Figure 7c

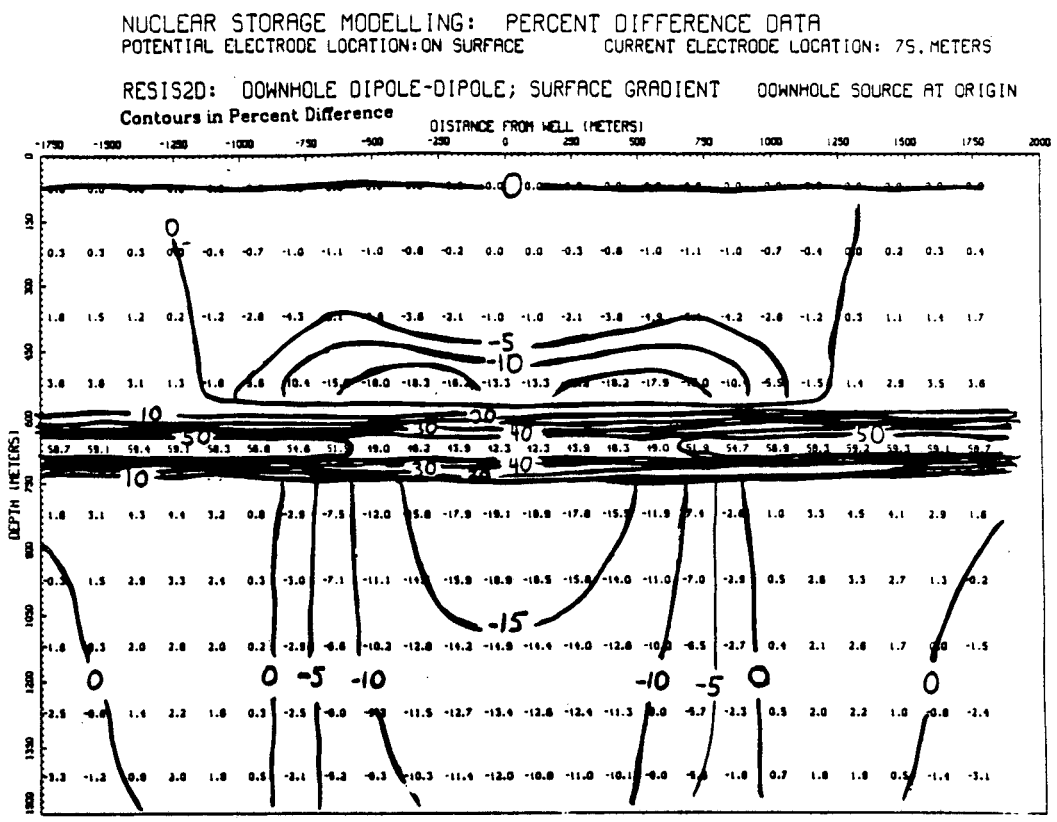

Figure 7d

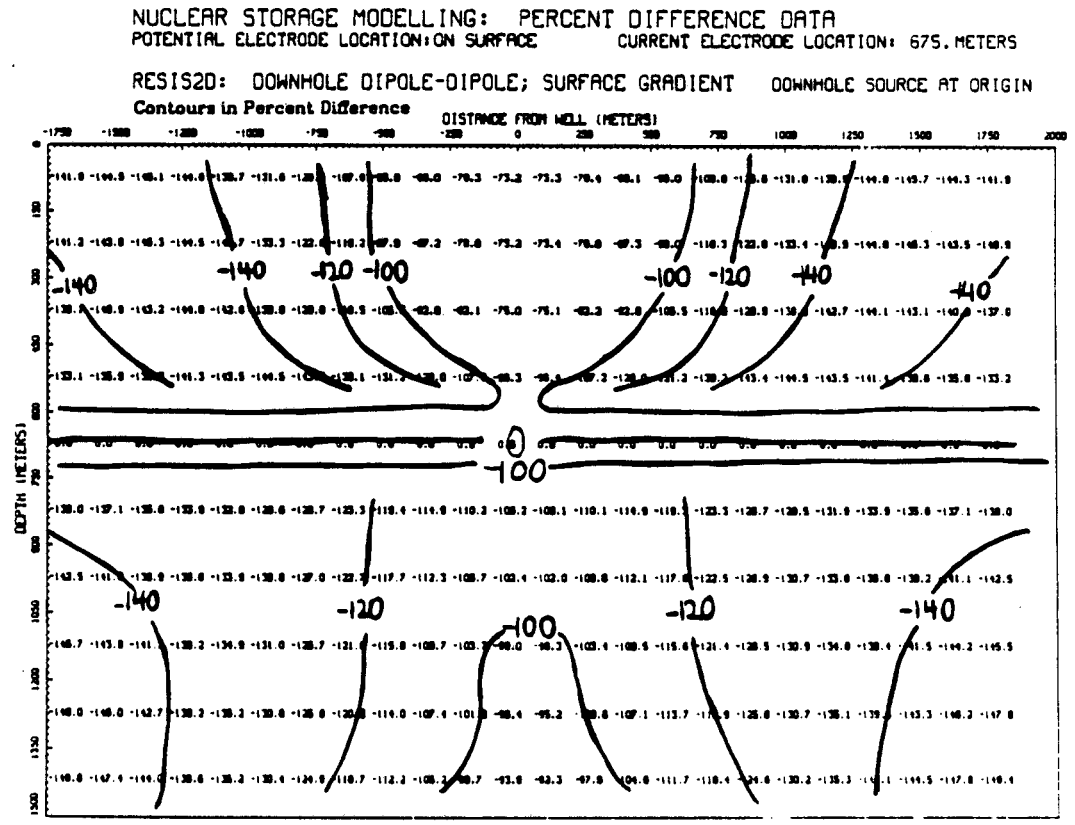

Figure 7e

NUCLEAR STORAGE MODELLING: APPARENT RESISTIVITY DATA
DIPOLE-DIPOLE SURFACE SURVEY
RESIS2D: COND. SURFACE ZONES OVER RES. REPOSITORY

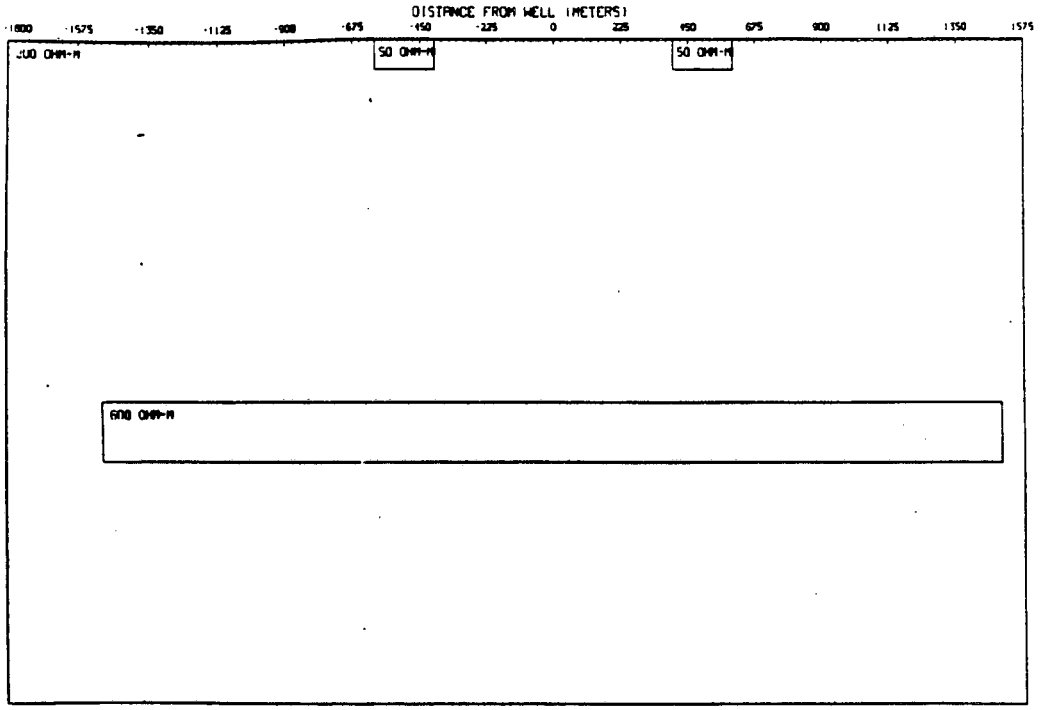

Figure 8a

NUCLEAR STORAGE MODELLING: PERCENT DIFFERENCE DATA
DIPOLE-DIPOLE SURFACE SURVEY
REFERENCE RESISTIVITY VALUE: 200.0OHM-METER
RESIS2D: COND. SURFACE ZONES OVER RES. REPOSITORY

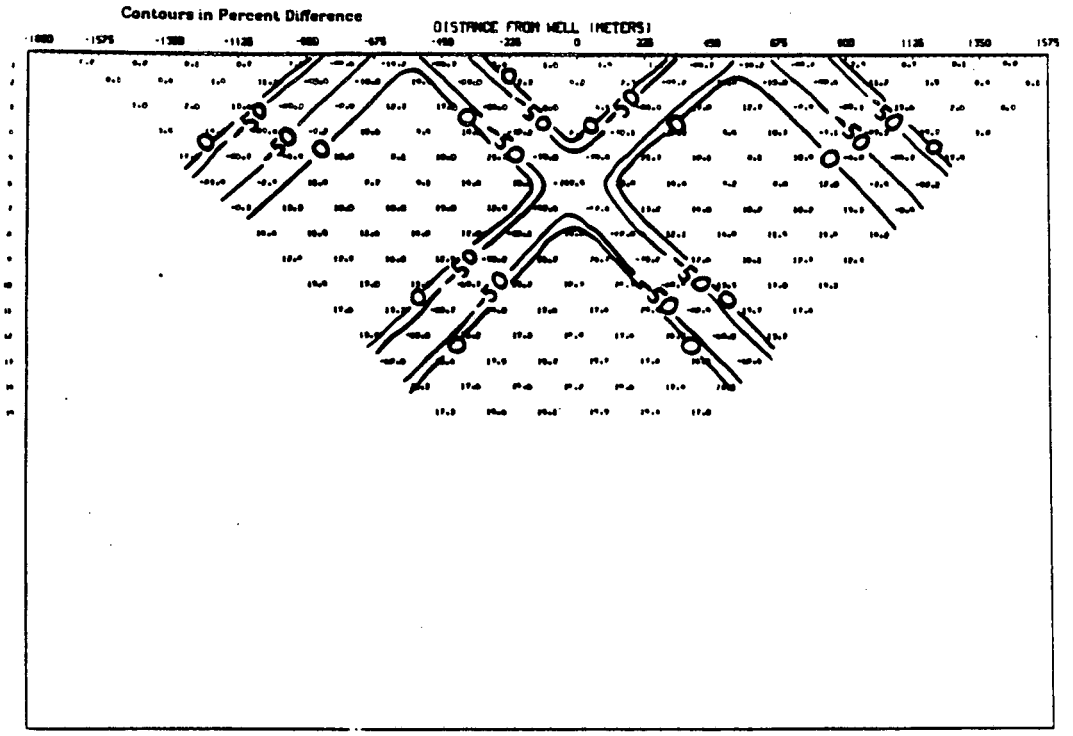

Figure 8b

NUCLEAR STORAGE MODELLING: APPARENT RESISTIVITY DATA
POTENTIAL ELECTRODE LOCATION: ON SURFACE

RESIS2D: COND. SURFACE ZONES OVER RES. REPOSITORY DOWNHOLE SOURCE AT ORIGIN

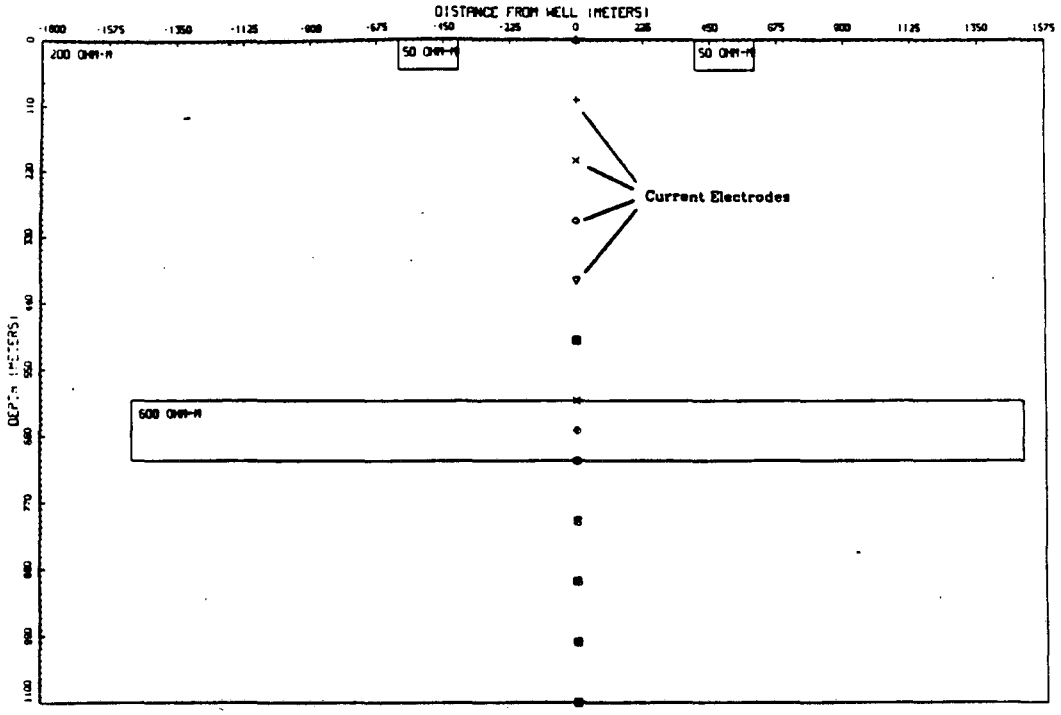

Figure 9a

NUCLEAR STORAGE MODELLING: PERCENT DIFFERENCE DATA
POTENTIAL ELECTRODE LOCATION: ON SURFACE REFERENCE RESISTIVITY VALUE: 200.0 OHM-METER
PERCENT DIFFERENCE = ((C2-C1)/C2)*100
RESIS2D: COND. SURFACE ZONES OVER RES. REPOSITORY DOWNHOLE SOURCE AT ORIGIN

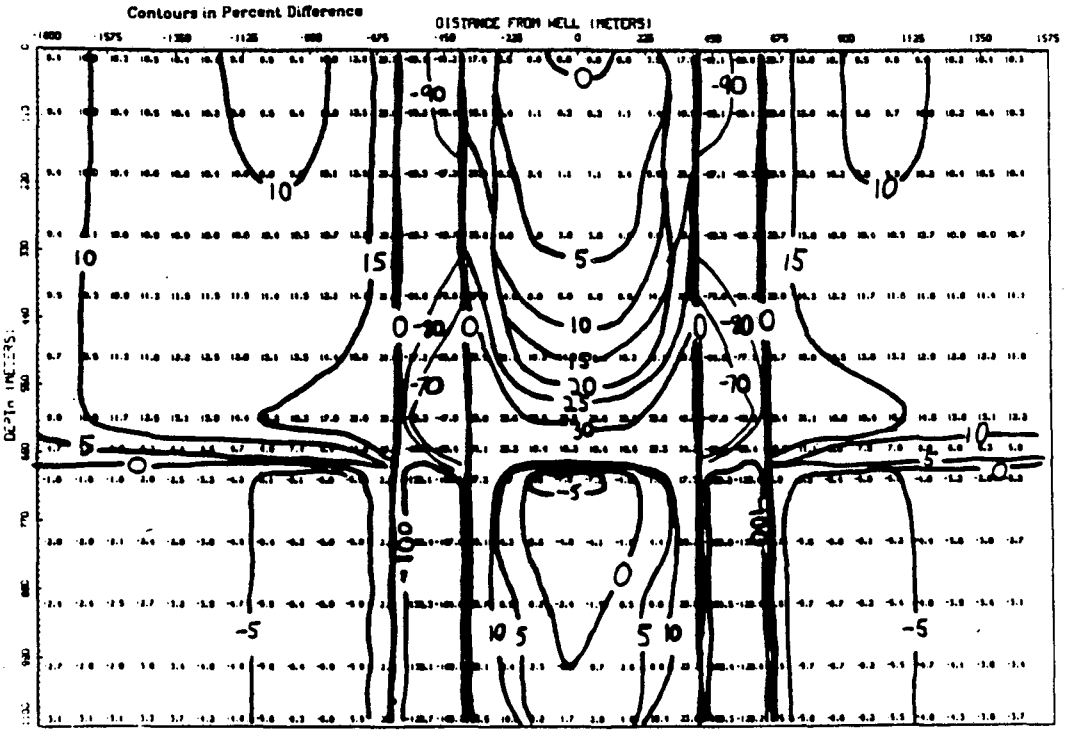

Figure 9b

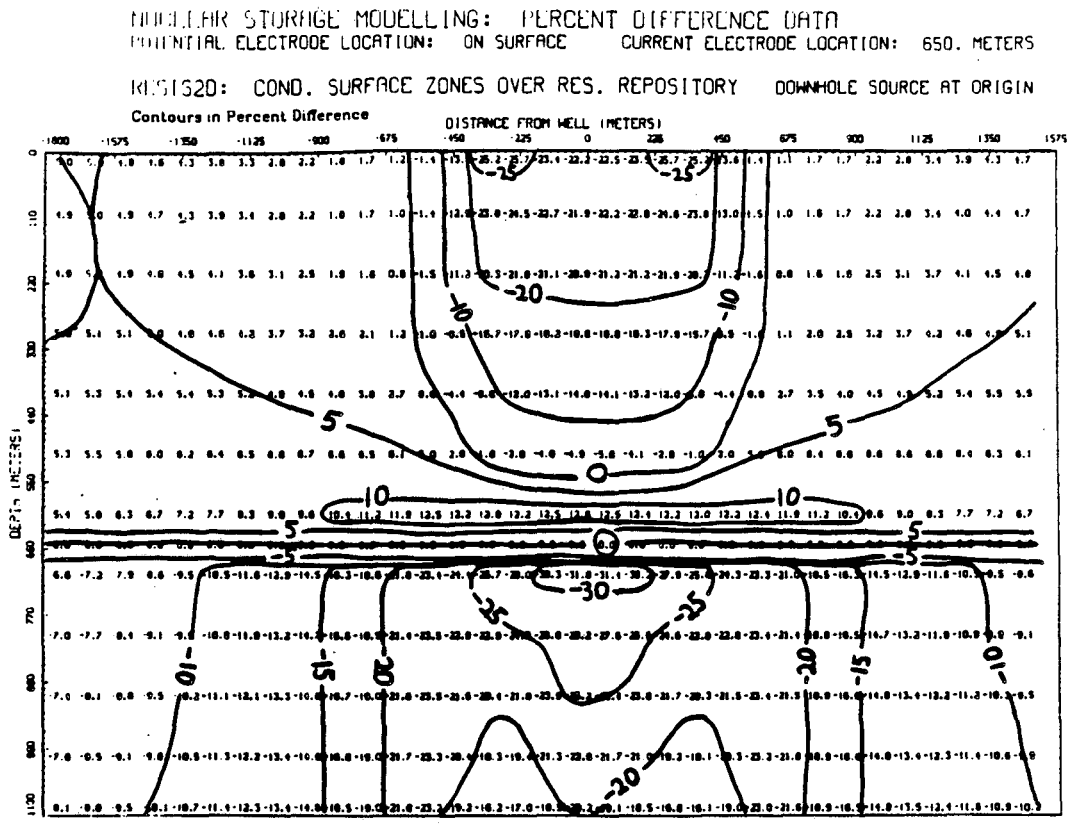
NUCLEAR STORAGE MODELLING: PERCENT DIFFERENCE DATA
POTENTIAL ELECTRODE LOCATION: ON SURFACE CURRENT ELECTRODE LOCATION: 650. METERS
RESI32D: COND. SURFACE ZONES OVER RES. REPOSITORY DOWNHOLE SOURCE AT ORIGIN
Contours in Percent Difference
DISTANCE FROM HELL (METERS)
DEPTH (METERS)

Figure 9c

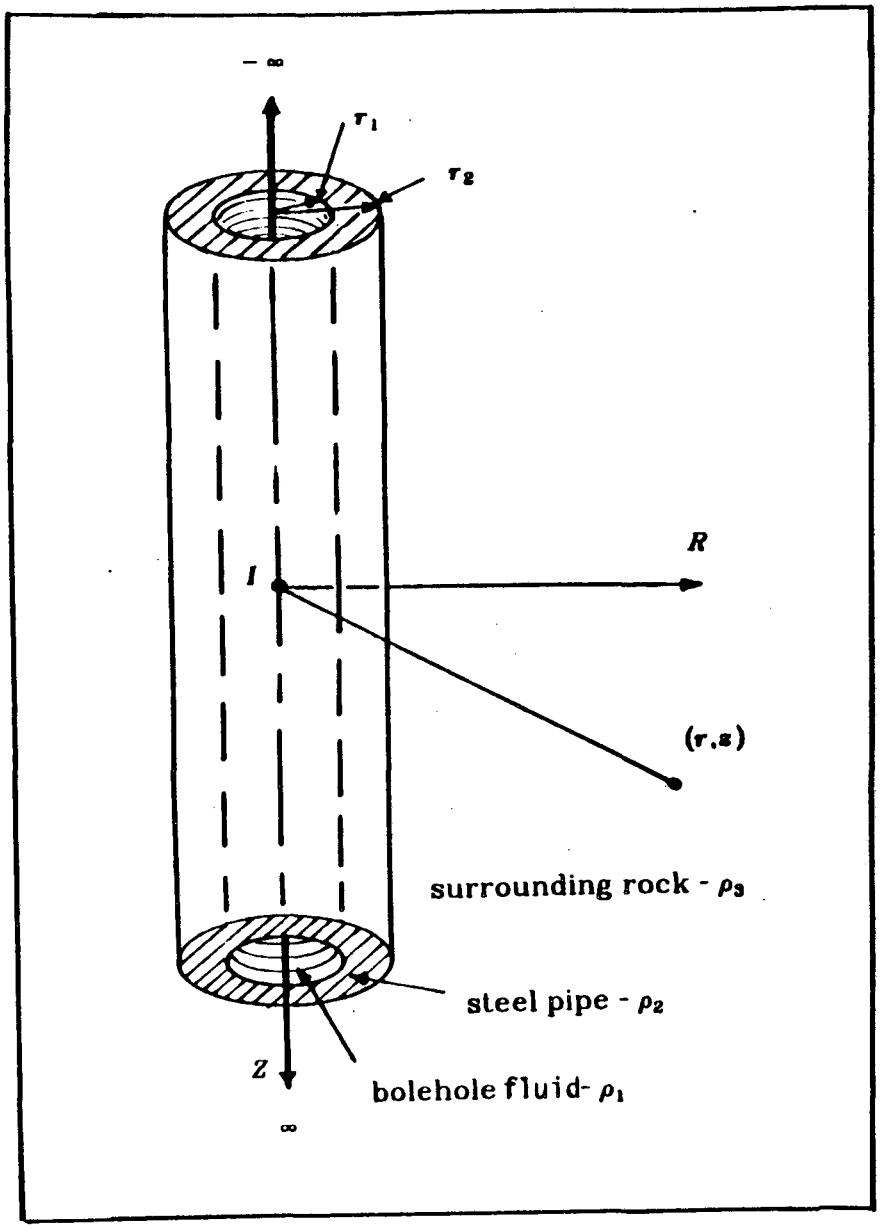

Figure 10a

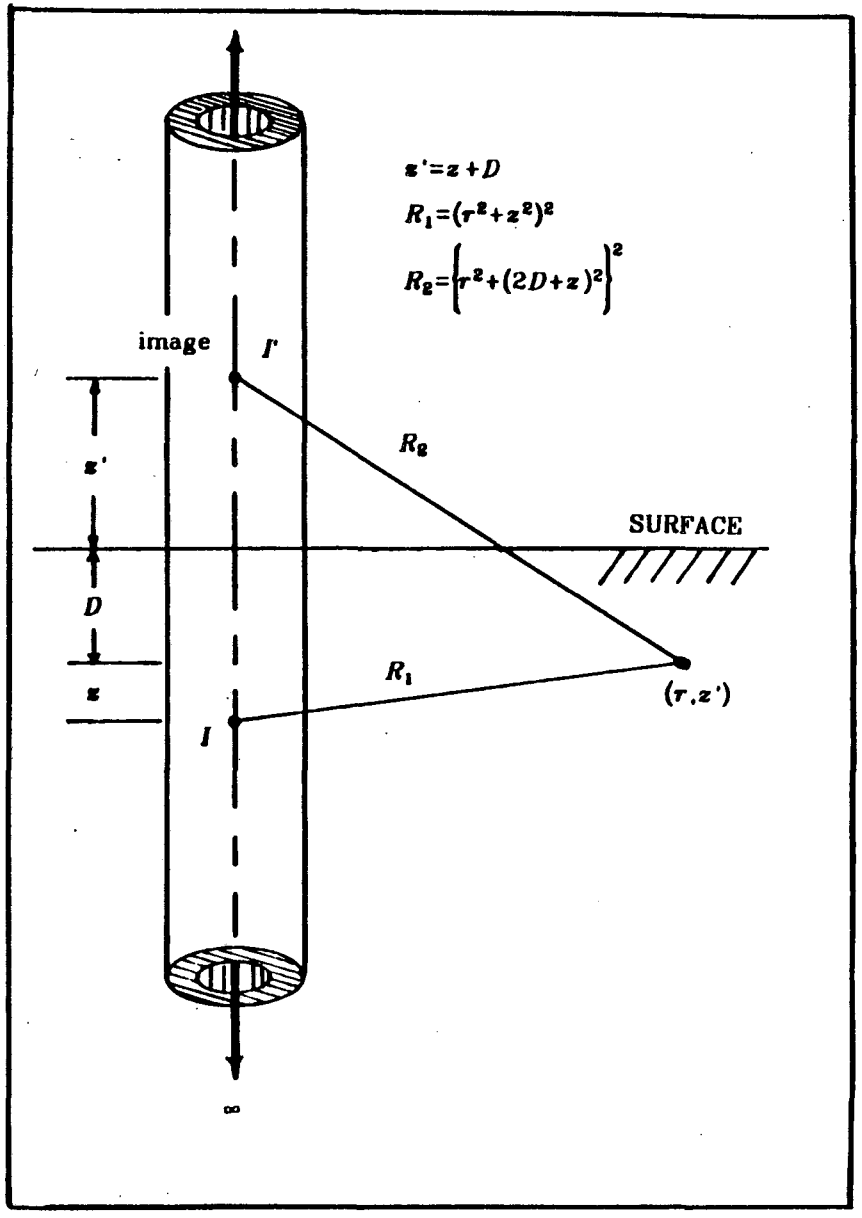

Figure 10b

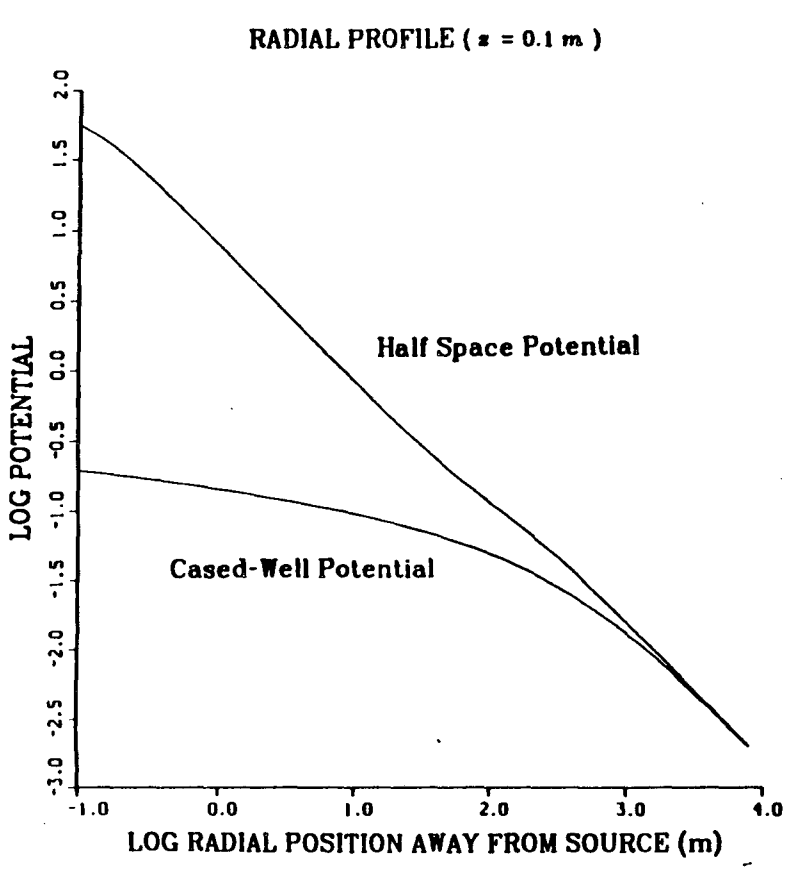

Figure 11a

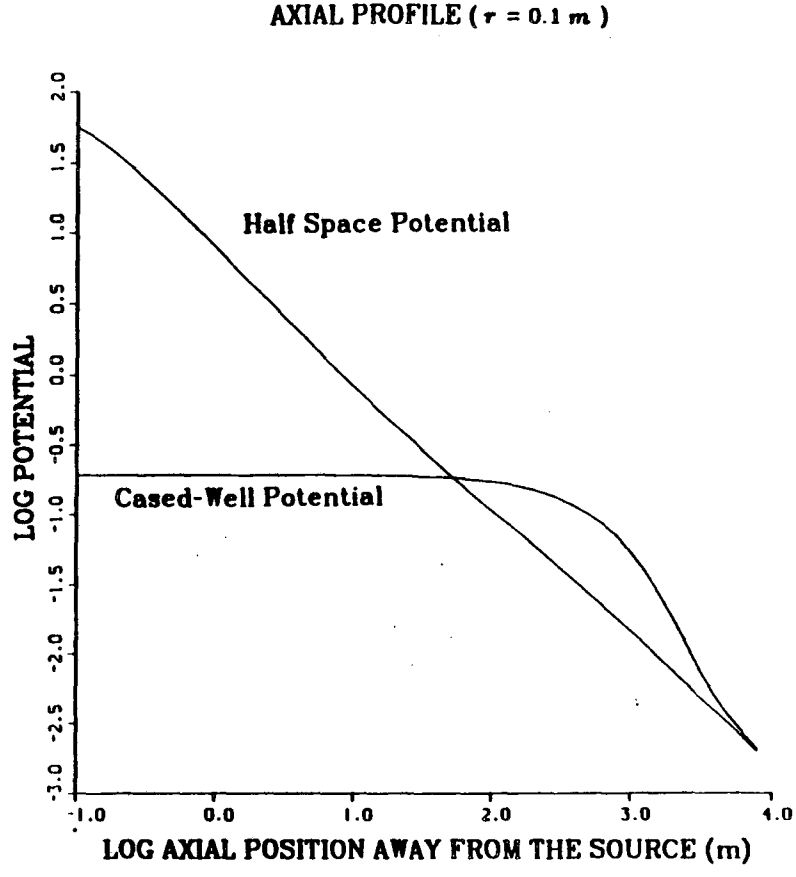

Figure 11b

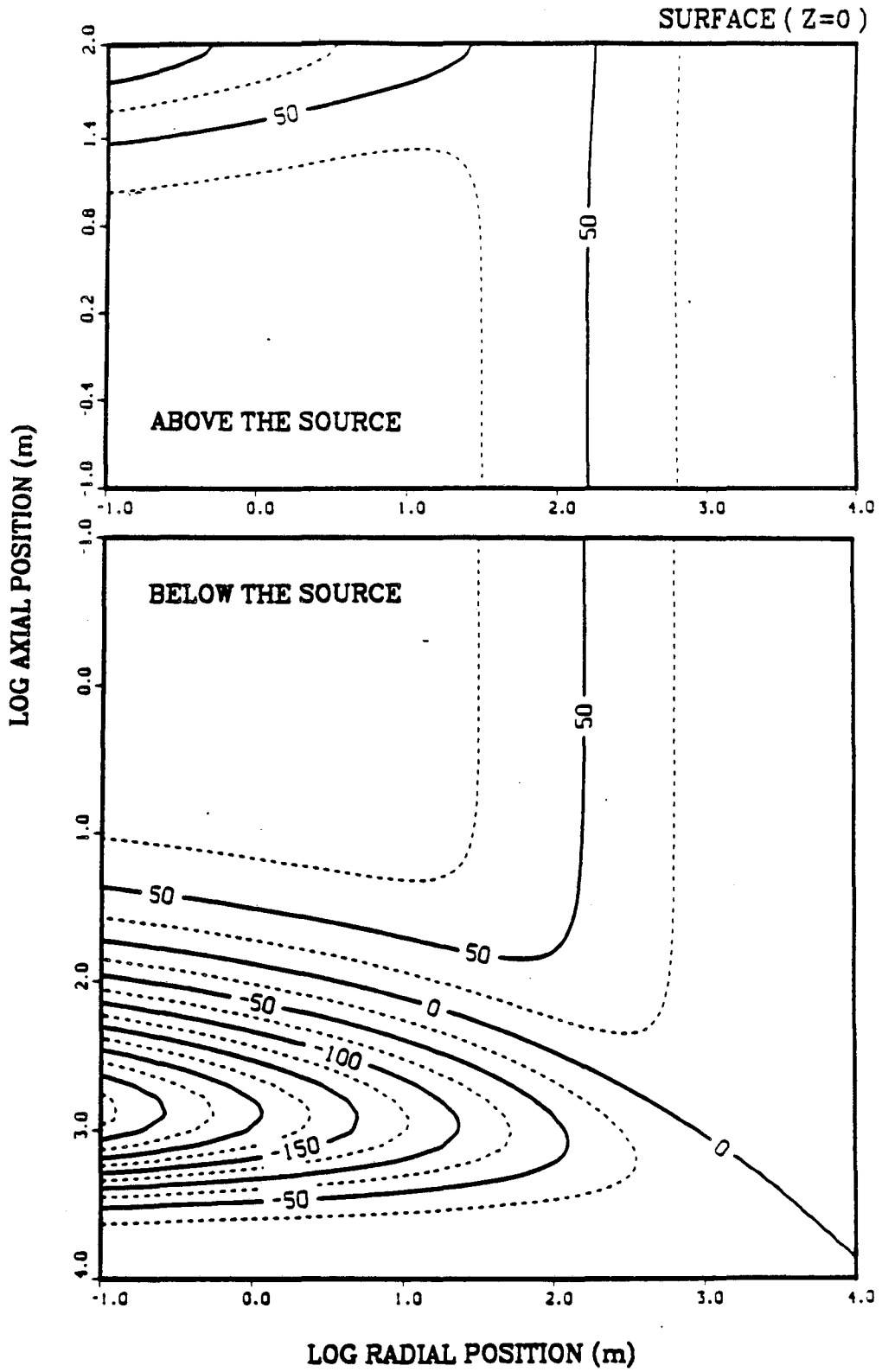
SURFACE (Z=0)
ABOVE THE SOURCE
BELOW THE SOURCE
50
50
50
50
0
-50
-100
-150
-50
0
LOG AXIAL POSITION (m)
LOG RADIAL POSITION (m)
2.0
1.4
0.8
0.2
-0.4
-1.0
0.0
1.0
2.0
3.0
4.0

Figure 12

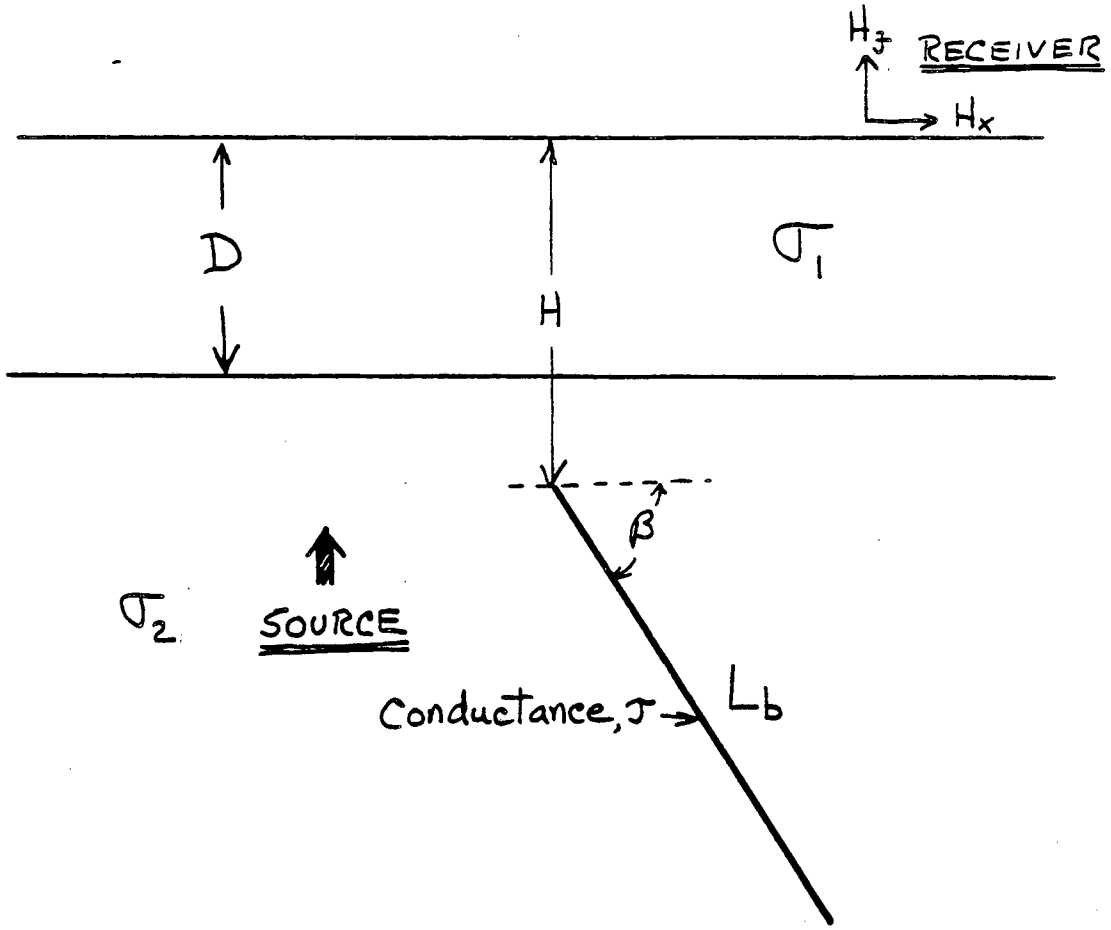
H_z
RECEIVER
H_x
D
H
σ_1
β
σ_2
SOURCE
Conductance, τ
L_b

Figure 13

Figure : 3-D view of the magnetic anomaly from sheet conductor

X-component of the anomaly, .V.E.D. source

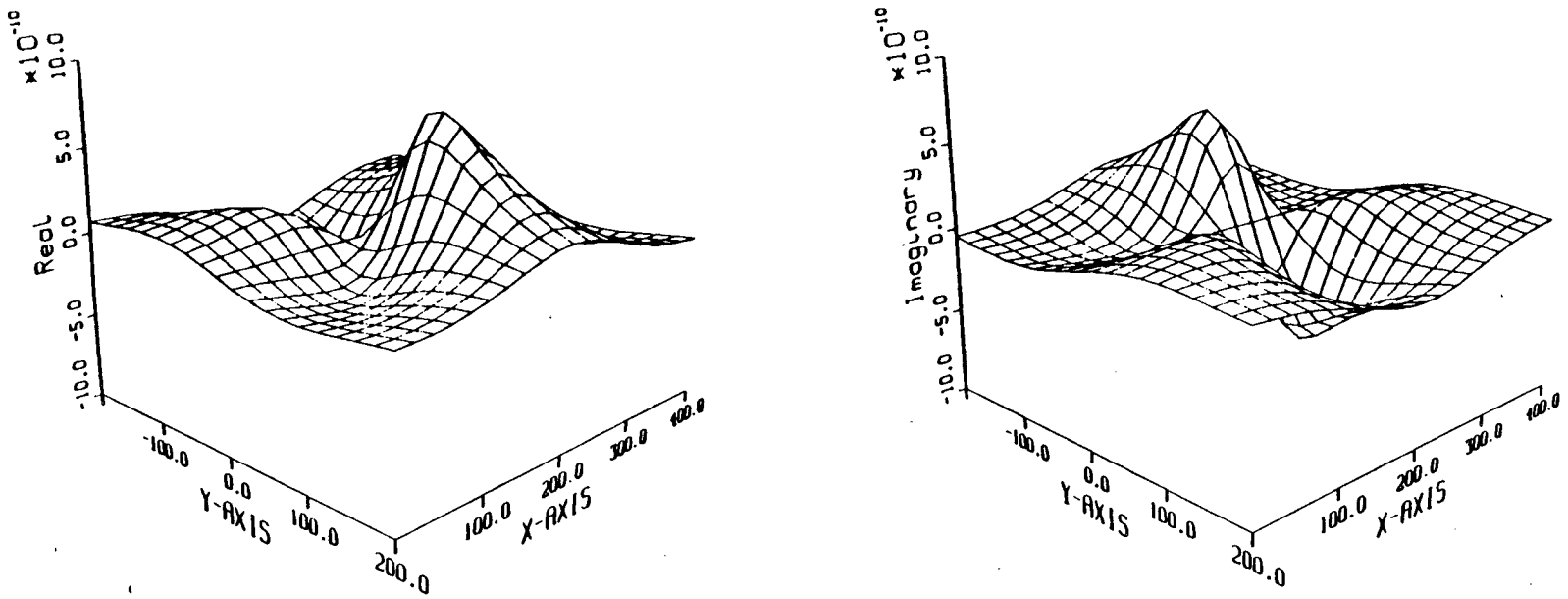

Figure 14

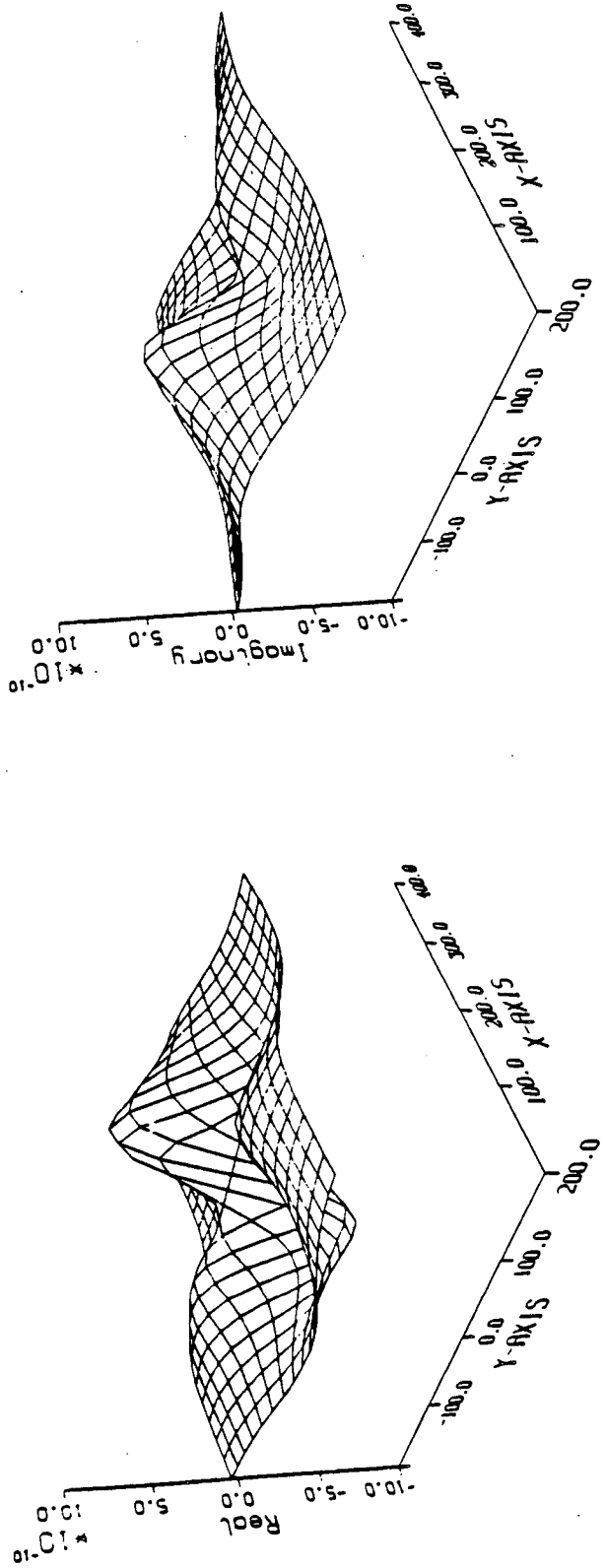

Figure : Y-component of the anomaly, V.E.D. source

Figure 15

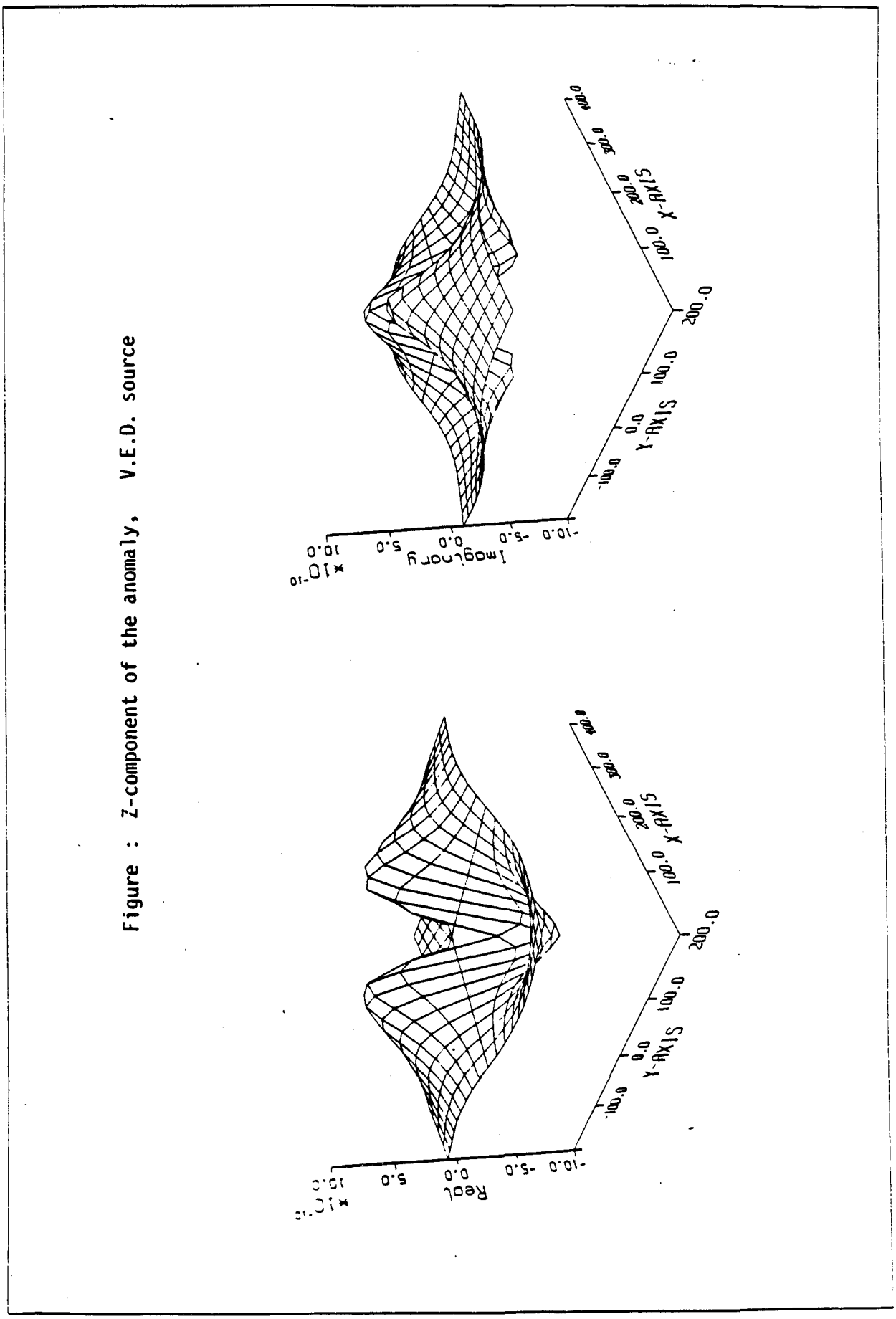
Figure : Z-component of the anomaly, V.E.D. source
Real
Imaginary
x-AXIS
y-AXIS
-10.0
-5.0
0.0
5.0
10.0
-100.0
0.0
100.0
200.0

Figure 16

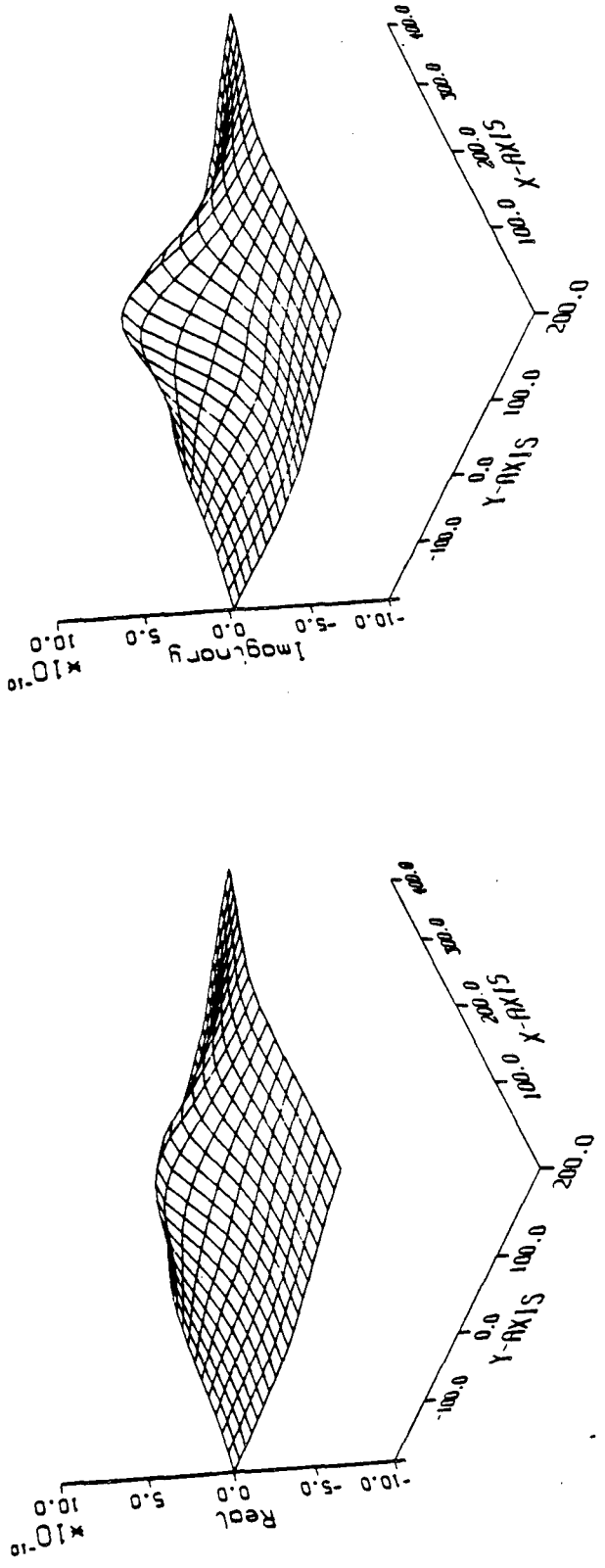

Figure : X-component of the anomaly, V.M.D. source

Figure 17

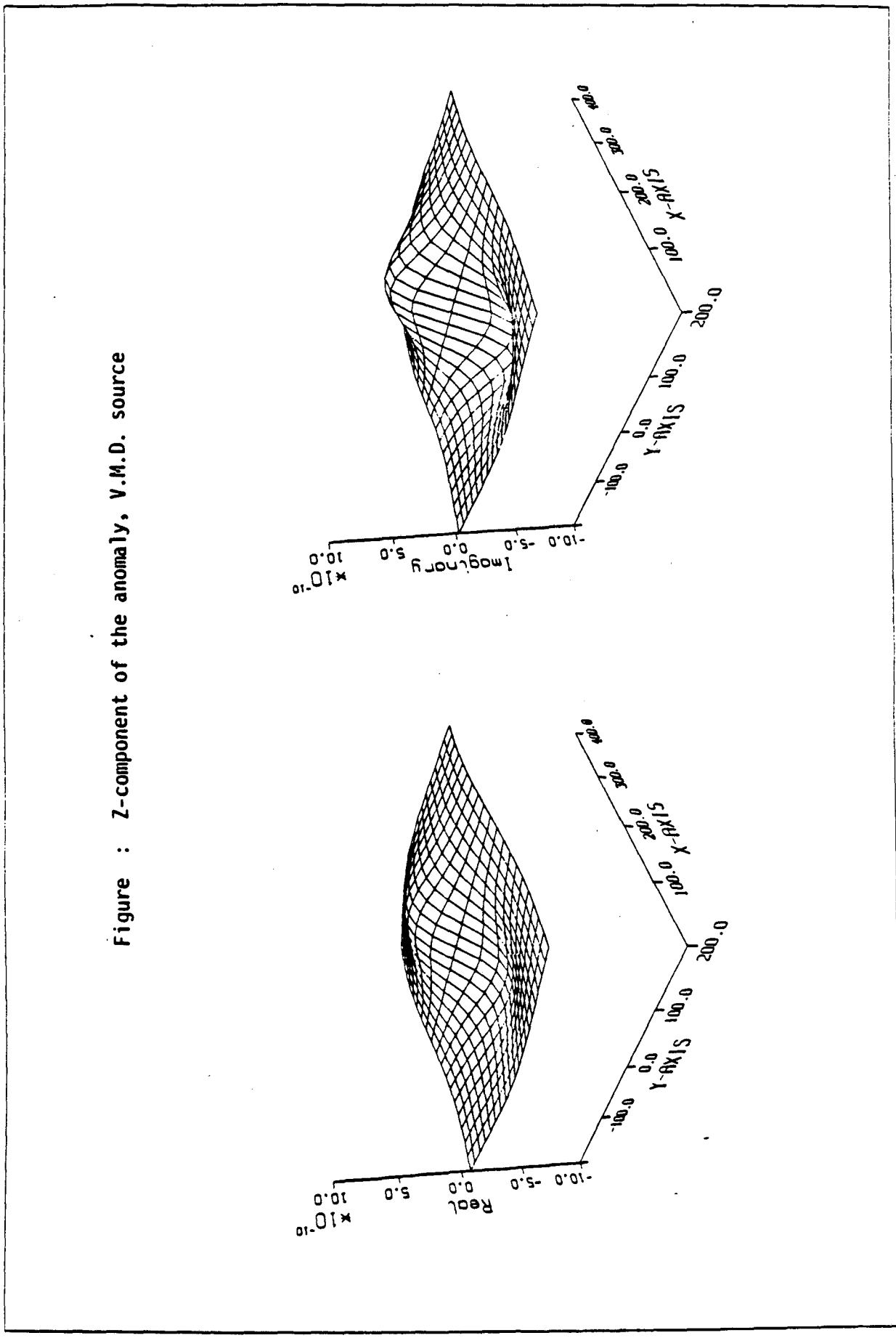
Figure : Z-component of the anomaly, V.M.D. source
Imaginary
Real
X-AXIS
Y-AXIS
x10^-10
10.0
5.0
0.0
-5.0
-10.0
200.0
100.0
0.0
-100.
-200.

Figure 18

LAWRENCE BERKELEY LABORATORY
TECHNICAL INFORMATION DEPARTMENT
UNIVERSITY OF CALIFORNIA
BERKELEY, CALIFORNIA 94720